PALEOCEANOGRAPHY, VOL. 10, NO. 6, PAGES 1011-1045, DECEMBER 1995

Constraints from paleotracer data on the North Atlantic circulation during the last glacial maximum

Pascal LeGrand[1] and Carl Wunsch

Center for Meteorology and Physical Oceanography, Department of Earth, Atmospheric, and Planetary Sciences
Massachusetts Institute of Technology, Cambridge

Abstract. We investigate the extent to which the paleotracers, $\delta^{13}C$ and $\delta^{18}O$, constrain the North Atlantic Ocean general circulation during the last glacial maximum (LGM). The distinction is made in this work between the depiction of water mass distributions and the inference of the oceanic circulation. The $\delta^{13}C$ data indicate that water masses formed in the North Atlantic and in the Southern Ocean were distributed differently during the LGM, but the extent of the differences cannot be quantified because of uncertainties in the end-member composition. Reasonable choices of values for the end-members produce volumes of Lower North Atlantic Deep Water (NADW) significantly smaller than in the modern Atlantic, in agreement with previous studies. To explore the range of circulations consistent with this water mass distribution, a coarse resolution inverse model of the North Atlantic is constrained with $\delta^{13}C$ and $\delta^{18}O$ paleodata. The model shows that the glacial period tracer distribution is fully consistent with the circulation rates estimated for the modern ocean. However, the paleodata are also consistent with a circulation rate of one-half the modern flux of NADW, and indeed there are an infinite number of rates of deep water movement that are possible. To remove this ambiguity, the central need is for a data type capable of setting the overall rates of water movement, i.e., a "clock", such as that provided by geostrophy or a well-sampled radioactive tracer.

1. Introduction

The oceanic thermohaline circulation apparently plays a major role in climate, and paleoceanographic data are among the few observations available for understanding the circulation in the past. Previous studies have interpreted differences in the tracer distribution during the last glacial maximum (LGM) from their present values in terms of changes in the fluxes of deep water. *Boyle and Keigwin* [1982, 1987], *Curry et al.* [1988], and *Duplessy et al.* [1988] used cadmium (Cd) and carbon 13 ($\delta^{13}C$) tracers to suggest a reduced flux of North Atlantic Deep Water (NADW) during the LGM. These studies rely on the assumption that changes in the water mass distribution implied by the tracers reflect changes in the intensity of the ocean circulation. This assumption, although plausible, has yet to be demonstrated to be correct.

The objective of this work is to understand the relation existing between water mass distribution, as deduced from paleotracer data, and the ocean circulation. We assume that the modern tracer distribution and the LGM tracer distribution represent two distinct steady states of the ocean. Making inferences about circulations supporting each tracer distribution is distinguished from the much more complex question of determining how the ocean switches from one state to the other. Modeling the glacial-interglacial transition would require a database depicting the oceanic state over the period of transition, and such data are only slowly emerging [*Sarnthein et al.*, 1994].

In this paper, we (1) compare the actual property distributions in the LGM and modern oceans and (2) use inverse models of both the glacial and the present-day oceans to examine quantitatively the implications of $\delta^{13}C$ and $\delta^{18}O$ tracers for the variation of the general circulation.

2. The Glacial and Modern Water Mass Distributions

A number of authors [*Boyle and Keigwin*, 1987; *Duplessy et al.*, 1988; *Boyle*, 1992; *Lohmann and Lohmann*, 1994] have demonstrated that a different distribution of water masses existed in the Atlantic Ocean at the LGM. The $\delta^{13}C$ maximum, characteristic of NADW in the modern South Atlantic, is not observed in the glacial Atlantic (Figure 1). High values of $\delta^{13}C$, however, can be traced back to the north of the Atlantic basin [*Sarnthein et al.*, 1994], and formation of NADW probably did not stop during the LGM. *Boyle and Keigwin* [1987] and *Duplessy et al.* [1988] suggested that the bulk of NADW may have lain at shallower depths during the last ice age, thereby shifting the high $\delta^{13}C$ values to intermediate depths. With the overlying thermocline waters also characterized by high $\delta^{13}C$ values [*Slowey and Curry*, 1992], NADW would no longer have appeared as a local $\delta^{13}C$ maximum in the glacial Atlantic. Another difference between modern and glacial water masses is that bottom waters were more depleted in $\delta^{13}C$ during the LGM than today, and vertical differences of

[1]Now at Institut Français de Recherche pour l'Exploitation de la Mer, Centre de Brest, Plouzané, France.

Paper number 95PA01455.
0883-8305/95/95PA-01455$10.00

$\delta^{13}C$ were larger. That $\delta^{13}C$ values were globally lower by about 0.3 ‰ [*Curry et al.*, 1988] can partly explain the lower bottom water values but not the increased vertical differences. A plausible explanation for these increased vertical differences is that Antarctic Bottom Water (AABW) extended farther north during the LGM, at the expense of Lower NADW [*Boyle and Keigwin*, 1982; 1987; *Duplessy et al.*, 1988; *Oppo and Lehman*, 1993; *Sarnthein et al.*, 1994]. The intermediate depth to bottom $\delta^{13}C$ differences would have then been larger because AABW is characterized by lower $\delta^{13}C$ values than NADW.

This redistribution of the water masses is plausible, but to quantify it, NADW and AABW must be defined. In the modern ocean, NADW appears clearly in a latitudinal section of $\delta^{13}C$ as the region delimited by relatively steeper $\delta^{13}C$ gradients (roughly the region enclosed by the 0.7 ‰ contour in Figure 1a). Thus one approach to identifying the LGM water mass distribution is to examine similar reconstructions of the latitudinal distribution of $\delta^{13}C$ in the glacial Atlantic.

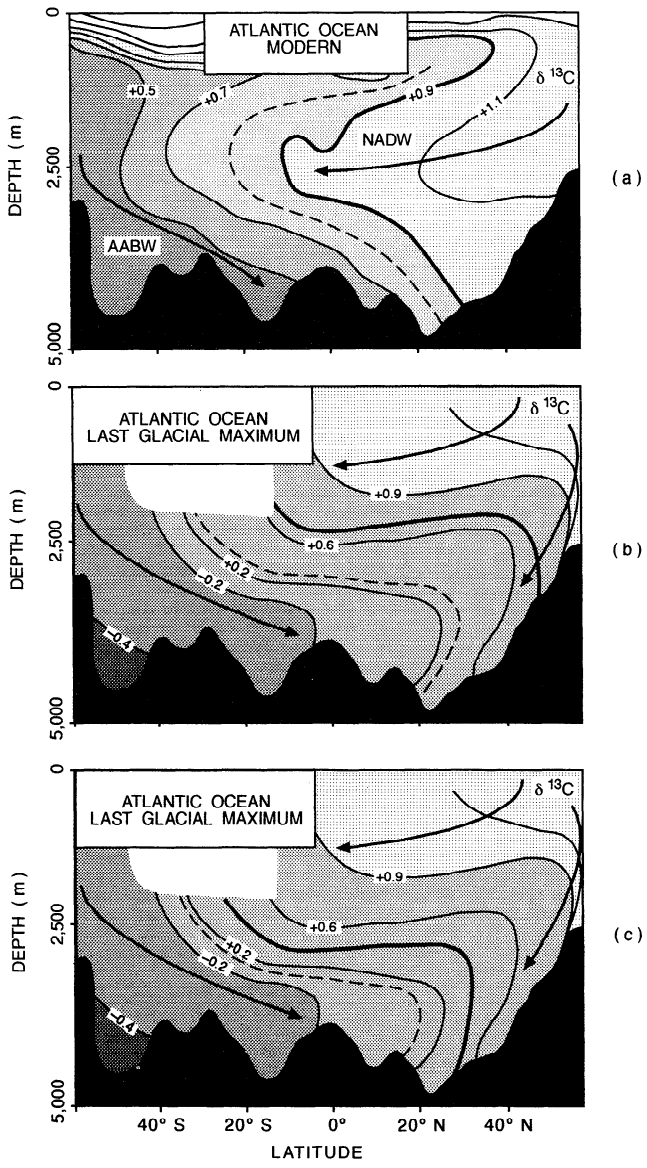

The $\delta^{13}C$ and $\delta^{18}O$ data for the LGM deep ocean are obtained by measuring the isotopic composition of benthic foraminifera tests preserved in the sediments. Benthic foraminifera live at the bottom of the ocean, and it is necessary to combine data sampled at different bottom depths to infer the vertical distribution of $\delta^{13}C$ and $\delta^{18}O$. An approach to reconstruction of latitudinal distributions of paleotracers is to collapse onto a single section observations originating from a relatively narrow longitude band. *Sarnthein et al.* [1994] show that a meridional section of $\delta^{13}C$ in the modern ocean reconstructed by collapsing all the core top data from the eastern Atlantic is consistent with direct measurements in the water column, within an error bar of less than 0.2 ‰. The distribution of sediment cores in the north Atlantic for which LGM benthic $\delta^{13}C$ and $\delta^{18}O$ values are available (Figure 2) shows that there are few cores between 500 and 2500 m depths, partly because of the lack of topographic features reaching these depths away from the continental margins and the Mid-Atlantic Ridge. Below 2500 m depth, there are more data available, but most of these are concentrated in the eastern Atlantic. There are only a few data along the American continental margin, where the strongest currents are expected.

The first attempt to contour a $\delta^{13}C$ section in the LGM eastern Atlantic was apparently that of *Duplessy et al.* [1988]. Their reconstruction suggests that the LGM water mass distribution was quite different from the modern ocean distribution, with NADW being replaced by a small and shallow mass of $\delta^{13}C$-rich water, which (following *Boyle and Keigwin* [1987]) they called Glacial North Atlantic Intermediate Water. The glacial deep Atlantic was filled with $\delta^{13}C$-depleted water of southern origin which they called Southern Ocean Water.

In this work, we use a more recent reconstruction produced by *Labeyrie et al.* [1992] from the same data as used by *Duplessy et al.* [1988]. This reconstruction also indicates a shift

Figure 1. (a) Water mass distribution in the modern Atlantic as inferred from $\delta^{13}C$ data (adapted from *Kroopnick* [1985]; these three figures are all redrawn from *Labeyrie et al.* [1992]; Reprinted from *Deep Sea Research*, vol. 32, P.M. Kroopnick, The distribution of ^{13}C of ΣCO_2 in the world oceans, pp. 57-84, Copyright 1985, and *Quaternary Science Reviews*, vol. 11, L.D. Labeyrie, J.-C. Duplessy, J. Duprat, A. Juillet-Leclerc, J. Moyes, E. Michel, N. Kallel, and N.J. Shackleton, Changes in the vertical structure of the North Atlantic Ocean between glacial and modern times, pp. 401-413, Copyright 1992, with kind permission of Elsevier Science Ltd., The Boulevard, Langford Lane, Kidlington OX5 IGB, UK.). Northern component waters are labeled NADW (North Atlantic Deep Water), and southern component ones are labeled AABW (Antarctic Bottom Water). At issue is the boundary between them. The dashed line is the position of water containing 50% contributions from each of the two end-members, and the thick line is the position of water composed of 2/3 from the northern end-member and 1/3 from the southern end-member. Here northern and southern end-members are 1.1 ‰ and 0.5 ‰, respectively. (b) Same as in Figure 1a, except for the last glacial maximum (LGM). Here northern end-member is 1.5 ‰ and the southern is -0.85 ‰. (c) Same as in Figure 1b, for the LGM ocean, but with different values for the end-members: 1.1 ‰ in the north and -0.85 ‰ in the south, which shifts the position of the 50% (dashed line) mixture water and 2/3 northern component (heavy solid line) water.

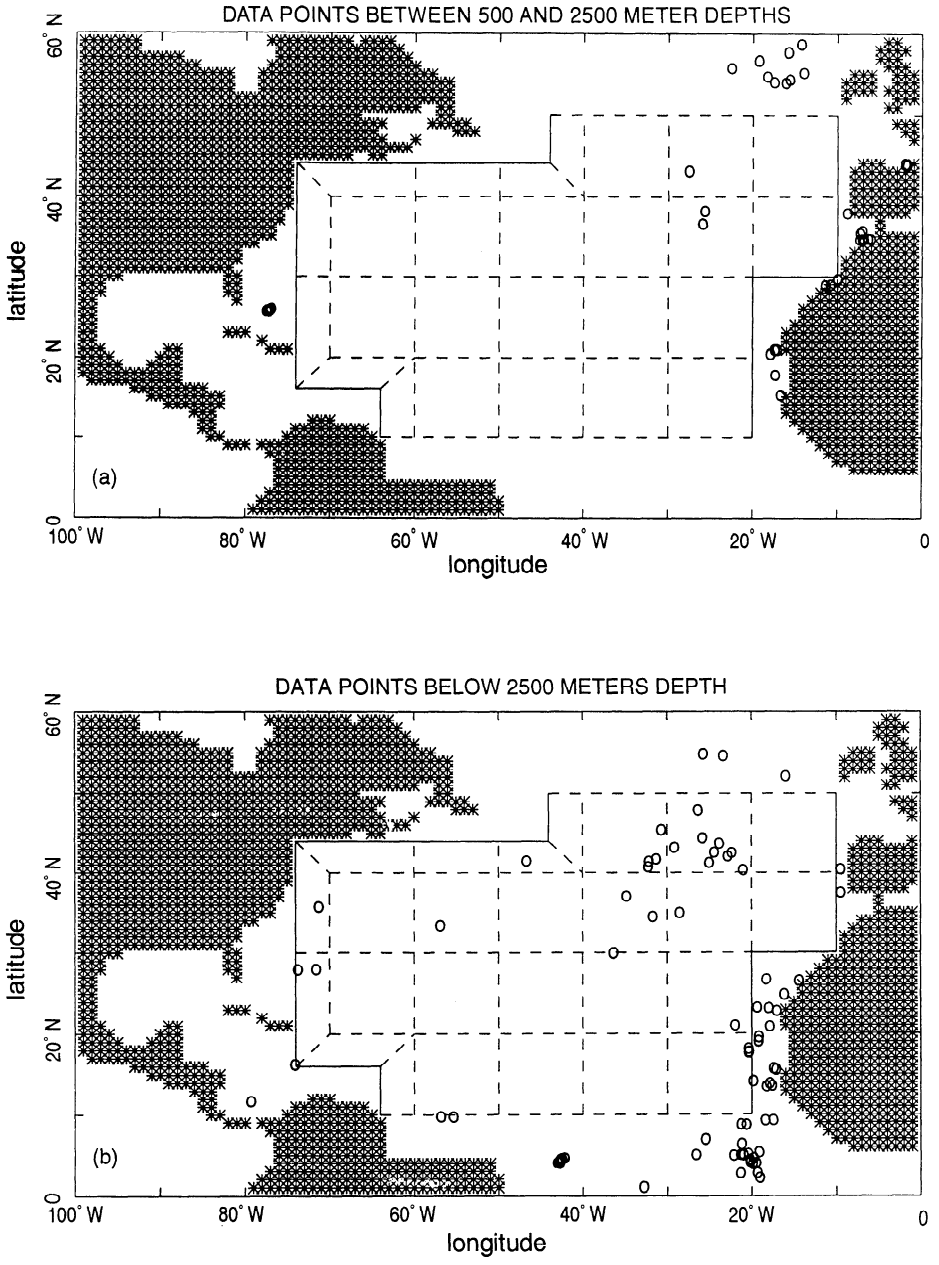

Figure 2. Location of deep-sea sediment cores for which $\delta^{13}C$ and $\delta^{18}O$ LGM measurements are available (top) between 500 m and 2500 m depth and (bottom) below 2500 m depth. The finite difference grid of the coarse resolution inverse model described in section 3-1 is superimposed. Tracer concentrations in the model are located at the corners of the volume elements. Volume transports are located at the center of the element interfaces. The westernmost series of boxes represent the Deep Western Boundary Current (DWBC).

in water mass volumes. The shading used by *Labeyrie et al.* [1992] suggests that the volumes delimited by the 0.9 ‰ isoline can be compared in Figures 1a and 1b and thus that the volume of the $\delta^{13}C$-rich water mass was smaller and shallower during the LGM. In reality, the end-member composition of the waters formed in the North Atlantic appears to have been different in the LGM and modern oceans [*Oppo and Lehman*, 1993]. Even if the water mass distribution in the LGM ocean were identical to that of today, one would expect the $\delta^{13}C$ "dye" in the water masses to have correspondingly different values. One must instead compare the positions of isolines defined in terms of the percentage of waters coming from the Southern Ocean and the North Atlantic.

For the glacial ocean, reasonable values for end-members of $\delta^{13}C$ are -0.85 ‰ at the southern end [*Charles and Fairbanks*, 1992] and 1.5 ‰ at the northern end [*Oppo and Lehman*, 1993]. A parcel of water made of 50% of each end-member then has a $\delta^{13}C$ of about (1.5 - 0.85) ÷ 2 = 0.3 ‰. For the modern ocean, reasonable values are 0.5 ‰ in the south and 1.1 ‰ in the north (Figure 1a). Thus, in the modern

ocean, a mixture of 50% of each end-member has a $\delta^{13}C$ of about (1.1 + 0.5) ÷ 2 = 0.8 ‰. The positions of the 50% lines (dashed lines) are similar in Figures 1a and 1b, and if NADW is defined as the water mass north of these lines, one obtains comparable volumes of NADW in the modern and glacial oceans.

A somewhat different picture emerges if one defines NADW as the water mass composed of more than 2/3 of the northern end-member. With the same end-member values as above, the 2/3 northern end-member + 1/3 southern end-member mixture corresponds to the 0.7 ‰ line in the glacial Atlantic and the 0.9 ‰ line in the modern Atlantic (thicker lines in Figures 1a and 1b). The volume located north of the 0.7 ‰ line in the LGM section (Figure 1b) is shallower than the volume located north of the 0.9 ‰ line in the modern section (Figure 1a), which suggests a reduced volume of Lower NADW and a greater northward extent of AABW during glacial times consistent with previous interpretations [*Boyle and Keigwin*, 1987; *Duplessy et al.*, 1988; *Labeyrie et al.*, 1992].

On the other hand, $\delta^{13}C$ values as high as 1.5 ‰ were not found below 1500 m in the LGM Atlantic [*Sarnthein et al.*, 1994; *Oppo and Lehman*, 1993], and hence one may argue that these values were significantly affected by $\delta^{13}C$-rich waters from the thermocline [*Slowey and Curry*, 1992]. In this case, the "true" value of the northern end-member may have been lower than 1.5 ‰. Assuming that this "true" value was as low as the modern northern end-member, 1.1 ‰, one finds in the LGM ocean that the 50% line is defined by the 0.1 ‰ contour and that the line delimiting the 2/3 northern end-member + 1/3 southern end-member mixture is defined by the 0.4 ‰ contour. The volumes delimited by these lines in Figure 1c are only slightly shallower than the corresponding volumes in Figure 1a (interglacial), which suggest that the volume of Lower NADW might have been only slightly reduced during the LGM, compared to the modern situation.

The uncertainty in the end-member composition could also result in an underestimate of the reduction of the volume of Lower NADW during the LGM. Indeed, the value of -0.85 ‰ for the southern end-member in the LGM Atlantic may be too negative [*Mackensen et al.*, 1993]. If instead one takes a value of -0.4 ‰ to characterize this end-member and a value of 1.5 ‰ to characterize the northern end-member, one obtains a value of 0.5 ‰ for the 50% mixture and a value of 0.9 ‰ for the 2/3 northern end-member + 1/3 southern end-member mixture. The isolines defined by these two mixtures are thus shallower than in the first example (with end-members of -0.85 ‰ and 1.5 ‰) and significantly shallower than in the modern ocean (compare the position of the 0.9 ‰ isoline in the LGM section (Figure 1b) with the position of the 0.9 ‰ isoline in the modern section (Figure 1a)). These relatively high end-member values therefore correspond to a much reduced volume of Lower NADW in the glacial ocean. Higher end-member values correspond to smaller volumes of Lower NADW.

A summary of the situation is that there is some evidence that the total volume of NADW present during the glacial pe-

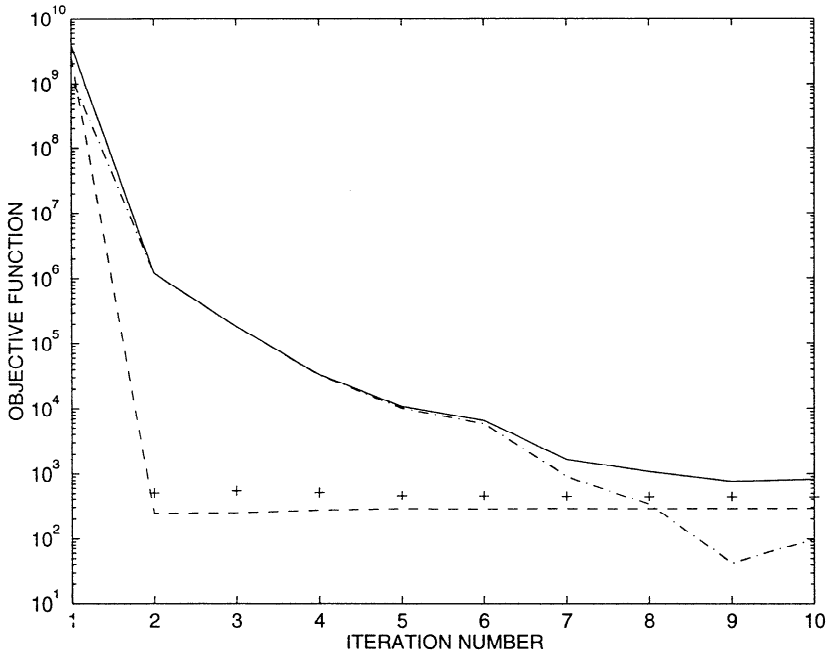

Figure 3. The objective function versus the number of iterations for the modern ocean run. Pluses represent the data misfit term $(\mathbf{x}-\mathbf{x}_0)^T \mathbf{C}_0^{-1} (\mathbf{x}-\mathbf{x}_0)$, and the initial data misfit is zero because the starting point of the minimization is the a priori solution, $\mathbf{x}_0$. Dotted-dashed line represents the contribution of the nonlinear physical constraints to the objective function, $\mathbf{f}(\mathbf{x})^T C_f^{-1} \mathbf{f}(\mathbf{x})$, and the dashed line represents the contribution of the linear physical constraints to the objective function, $(\mathbf{A}\mathbf{x}-\mathbf{b})^T \mathbf{C}_A^{-1} (\mathbf{A}\mathbf{x}-\mathbf{b})$. Solid line represents the objective function, which is the sum of the three preceding terms.

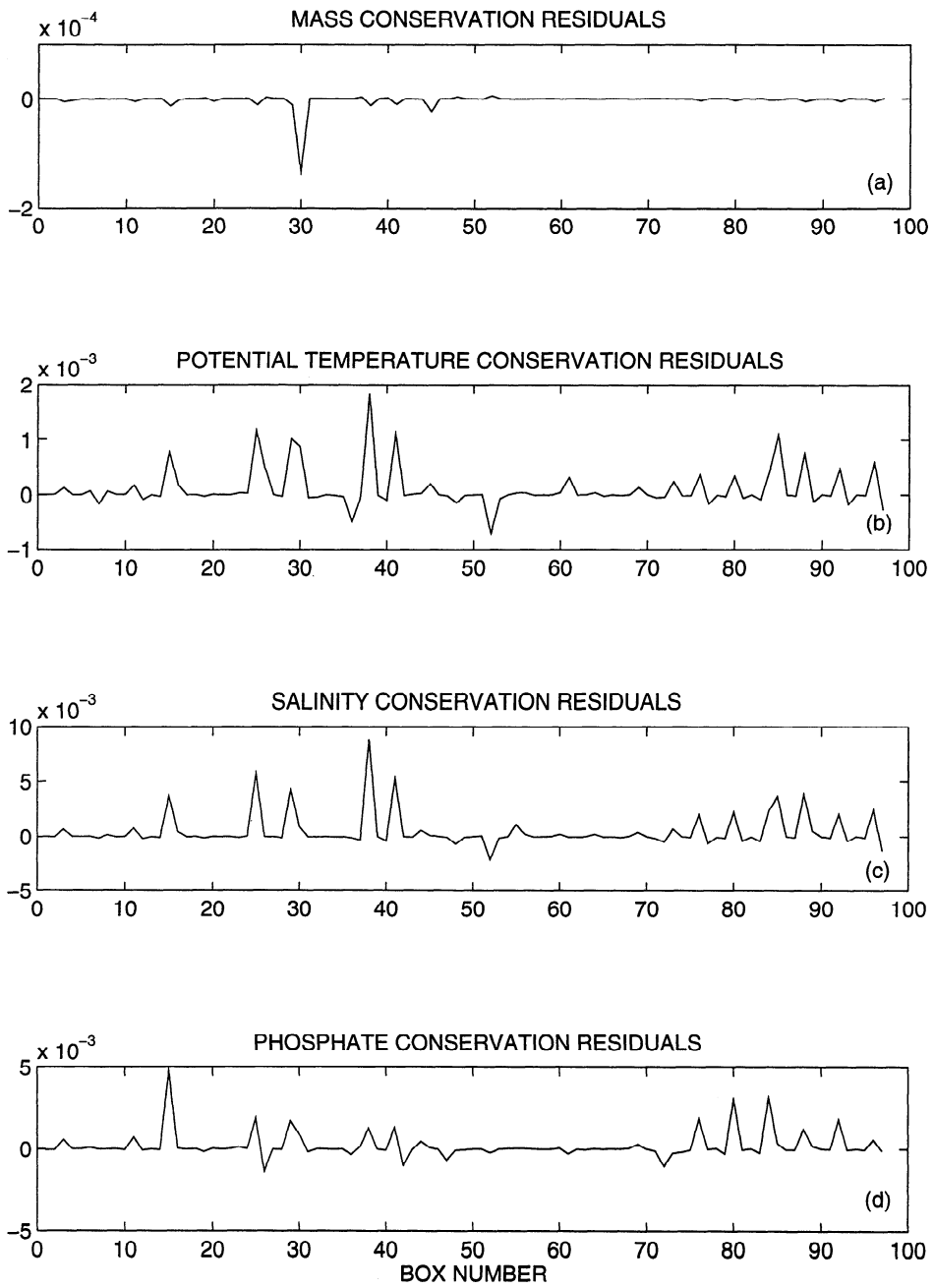

Figure 4. (a-d) Residuals in each volume element of the model after minimization, for the property conservation equations in the modern ocean run. There are 97 such elements (boxes). Conservation equation residuals are defined as the sum of the fluxes entering the box divided by the absolute value of the largest flux leaving or entering the box. (e-f) Residuals after minimization in the modern ocean run for the linear vorticity balance in each box where it is imposed and for the thermal wind balance at each section where it is imposed. The residuals are defined as the left-hand side minus the right-hand side of the equations, divided by the largest of those two terms.

riod was smaller than today, but the calculation is rendered uncertain because the end-member values corresponding to the regions of deep water formation are poorly constrained. One can question the range of water mass volumes that we find because it depends greatly on the range of end-member values. We took extreme end-member values to illustrate better the uncertainties associated with the volume reconstructions. Some of these values may be too extreme, such as -0.85 ‰ for the glacial southern end-member. If this value can be ruled out, then the range of possible water mass distributions will be narrowed. The important point, however, is that the water mass volume reconstructions will remain uncertain as long as the end-member values are not precisely determined. More data are needed close to the regions of deep water formation to

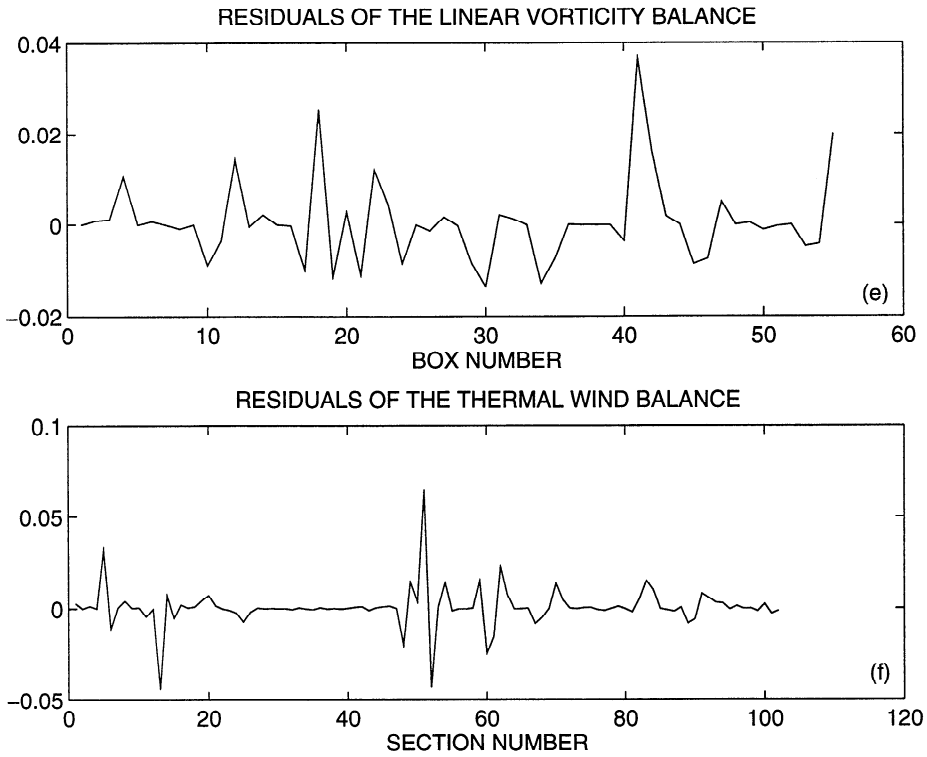

Figure 4. (continued)

quantify the differences between modern and glacial water mass distributions.

Higher vertical $\delta^{13}C$ differences in the LGM Atlantic than today (Figure 1) do not necessarily mean that the volumes of the various water masses were different. The larger differences could simply be due to a change in the preformed values of $\delta^{13}C$ which characterize the end-members. Preformed values of $\delta^{13}C$ in the Southern Ocean seem to have been lower, and preformed values of $\delta^{13}C$ in the North Atlantic seem to have been higher during the LGM than during interglacial times. This difference, by itself, can create $\delta^{13}C$ depleted bottom waters and $\delta^{13}C$ enriched intermediate waters in the North Atlantic and must explain part of the large $\delta^{13}C$ vertical differences observed in the glacial ocean.

3. Circulation Estimate for the LGM From Paleotracers and an Inverse Model

Despite the uncertainties on the end-member composition, water mass volumes indicated by $\delta^{13}C$ appear to have been at least somewhat different during the LGM. Previous authors have attributed these differences to circulation changes. It was hypothesized that the reduced volume of Lower NADW was due to a reduced rate of production of this water mass and that the greater volume of waters of northern origins at intermediate depths was due to an enhanced formation of intermediate waters in the glacial North Atlantic [*Boyle and Keigwin*, 1987; *Duplessy et al.*, 1988; *Oppo and Lehman*, 1993; *Sarnthein et al.*, 1994]. This circulation change scenario has be-

Table 1. Characteristic Times Associated With the Conservation Equation Imbalances in the Circulation Estimates Presented in This Paper

	Mass	Potential Temperature	Salinity	Phosphate or Carbon 13
Modern ocean reference circulation estimate	13	4	2	0.6
Paleocirculation estimate 1	7	3	620	4
Paleocirculation estimate 2	22	53	545	5
Modern ocean "phosphate-only" circulation estimate	31	6	28	1379

Characteristic times are given in millions of years. The conservation equation imbalances are integrated over the model domain. The characteristic time for mass conservation equations is the time the mass imbalances would take to double the volume of the model domain, and the characteristic time for the tracer conservation equations is the time the tracer imbalances would take to change the mean potential temperature over the model domain by 1°C, the mean salinity by 1, the mean phosphate concentration by 1 μmol/kg, and the mean $\delta^{13}C$ by 1 ‰.

come the conventional interpretation of the observed differences in the water mass distribution.

However, it is not obvious that changes in the water mass distribution can be interpreted in terms of changes in the oceanic circulation. The $\delta^{13}C$ is a passive tracer, and under the steady state assumption, the circulation must be consistent with the observed "standing crop". This means only that as long as the volume divergences of the tracer are in balance, the absolute fluxes are free to vary. Note in particular that an extreme circulation, no flow at all, is consistent with any distribution of $\delta^{13}C$ in the absence of biological activity.

In this section therefore we attempt to understand the range of circulation that is consistent with the LGM tracer distribution, by means of a coarse resolution inverse model of the deep Atlantic. The geochemical tracers $\delta^{13}C$ and $\delta^{18}O$ are used as constraints on the circulation during the LGM.

3.1. A Coarse Resolution Inverse Model of the North Atlantic

3.1.1. Model constraints. The inverse model we use includes a simplified representation of the physics of the ocean circulation: linear vorticity and thermal wind balance; conservation of mass, potential temperature, salinity; and a third tracer (phosphorus in the modern ocean and $\delta^{13}C$ in LGM runs). These physical constraints are commonly used in inverse modeling [*Wunsch*, 1978, 1985, 1989] and are introduced into the model as finite difference equations. The model domain is the deep North Atlantic from 10°N to 50°N (Figure 2) and from 1 km depth to the bottom. It is divided into volumes of 10° x 10° x 1 km, and conservation statements are written for each of these volumes. A series of 32 boxes is added to the western side of the model to simulate the Deep Western Boundary Current (DWBC). These boxes are treated in the same way as the interior boxes except that the linear vorticity balance is not imposed because one expects higher order physics in the DWBC [*Stommel and Arons*, 1960a, b]. There is no flow through the eastern and western boundaries, the Mid-Atlantic Ridge, and the bottom of the ocean. The Mid-Atlantic Ridge is crudely represented at depths below 3 and 4 km, and the deep eastern Atlantic is isolated from its western counterpart below 4 km depth.

The thermocline and the mixed layer are not explicitly modeled. For the LGM ocean, there are few data in the thermocline, and it is not clear whether $\delta^{13}C$, the main source of information, is reliably recorded by planktonic foraminifera in the mixed layer [*Keigwin and Boyle*, 1989]. Modeling the upper kilometer of the ocean would require the addition of several layers in the model and greatly increase the number of variables; as a result, it is postponed until more data become available in the thermocline. There are, however, exchanges of mass and tracer between the model domain and the upper ocean that are computed by the model.

The fluxes of water and tracer across 10°N, 50°N, and the 1 km depth level are treated as variables to be estimated. In other words, the model determines boundary conditions that are consistent with the interior data and physical constraints. The model domain is limited to the North Atlantic because the available data set lies predominantly in this region, and it is sufficiently large to estimate general circulation changes. Latitude 50°N is close to the regions of formation of NADW, and 10°N is sufficiently far south for the model to feel the influence of AABW. Indeed, a $\delta^{13}C$ meridional section in the modern ocean clearly shows bottom water depleted in ^{13}C north of the equator (Figure 1a). The LGM data are usually interpreted as a sign that AABW penetrated farther north then, and the influence of this water mass should be even more noticeable in LGM runs. In addition, limiting the study to the North Atlantic keeps the size of the problem tractable; there are about 850 variables and 1000 equations in the dynamical box model.

The very coarse resolution of the model appears to be all that is justified in view of the incomplete geographical coverage of the data set. Even on such a coarse resolution grid, there are many grid points which are not constrained by any observations, especially in the western Atlantic (Figure 2, top and bottom panels). As more data become available, some of the gaps will be filled, but there are areas in the ocean which will not be covered such as intermediate waters away from continental margins or below the calcium compensation depth where foraminifera shells dissolve. We seek oceanic circulations that are consistent with the LGM observations and with the model, and this objective can be achieved with the present coarse resolution. We also demonstrate below that the model is consistent with modern ocean data and produces a reasonable solution.

Mathematically, the model is similar to that of *Mercier* [1989]. However, unlike his model, temperature and salinity are treated as independent variables to produce density through an equation of state. For the sake of simplicity, a linearized equation is used, with coefficients determined every kilometer between 1 and 5 km depths from a linear regression of data from the *Fukumori et al.* [1991] atlas (see *LeGrand* [1994] for details.)

Let $\mathbf{x}$ be the vector of variables which completely defines the oceanic state in terms of the model and which is normally referred to as the "state vector". The present model representing advection of tracers by a large-scale ocean circulation has a state vector whose elements are the flow field and tracer field at each model grid point. The model, being a steady state one, can be written:

$$\mathbf{f}(\mathbf{x}) = 0 \tag{1}$$

where $\mathbf{f}$ is defined as the vector which contains the equation imbalances, such as, for instance, the mass imbalances in each volume element of the model. Here $\mathbf{f}$ is a nonlinear function of $\mathbf{x}$ because the tracer conservation equations are the product of mass transport terms by tracer concentration terms, both terms being variable in the model.

3.1.2. Combining model and observational constraints. The problem is to combine the available observations with the known physics as embodied in (1) to make a best estimate of the ocean circulation. Both model equations and the data contain errors, and any successful model/data combination must account for the relative accuracy of the different pieces of information.

Following the estimation literature, and, for example, the approach of *Mercier* [1986], define an objective function

$$J = (\mathbf{x}-\mathbf{x_0})^T \mathbf{C}_0^{-1} (\mathbf{x}-\mathbf{x_0}) + \mathbf{f}(\mathbf{x})^T \mathbf{C}_f^{-1} \mathbf{f}(\mathbf{x}) \tag{2}$$

where $\mathbf{x}_0$ is a prior estimate of the state vector, $\mathbf{C}_0$ is an estimate of the covariance of the uncertainty of that estimate, and $\mathbf{C}_f$ is the corresponding matrix for estimated errors in the model equations. In the present particular situation, some of the $\mathbf{x}_i$ are directly observed and the corresponding $(\mathbf{C}_0)_{ii}$ is the estimated observation error variance. For other elements, not directly observed, $\mathbf{x}_0$ is simply a plausible estimate; corresponding elements of $(\mathbf{C}_0)_{ii}$ are made sufficiently large that the initial estimate has little effect on the final solution. No off-diagonal elements of $\mathbf{C}_0$ are used.

The sources of error in the model, specified by $\mathbf{C}_f$, are many and difficult to quantify. These sources include the assumption of a steady state ocean, the coarse resolution, and oversimplified physics. Here, $\mathbf{C}_f$ is taken to be diagonal and mainly determined by trial and error, thus representing a set of curve-fitting weights rather than a statistical estimation procedure. In general, large weights (corresponding to small elements of $\mathbf{C}_f$) are used to impose mass conservation almost exactly. Smaller weights (corresponding to larger elements of $\mathbf{C}_f$) are used for the other equations, which are thus satisfied only ap-

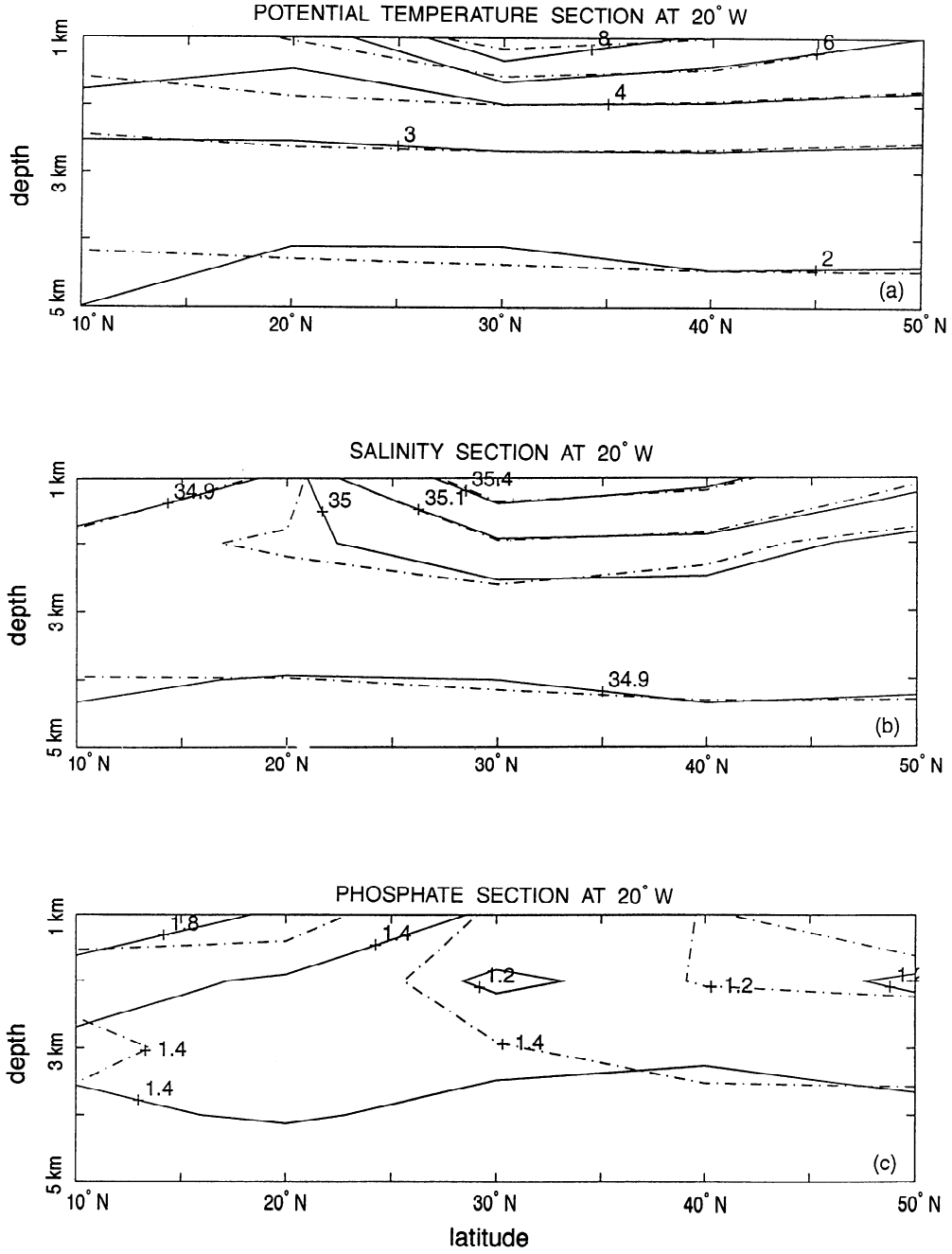

Figure 5. Meridional sections of potential temperature (in degrees Celsius), salinity (Practical Salinity Scale), and phosphate (micromoles per liter) in the modern ocean at 20°W. Solid lines represent the model estimates after optimization. Dotted-dashed lines represent the prior tracer distributions subsampled at each model grid point from the *Fukumori et al.* [1991] atlas.

proximately by the solution to the optimization problem. A quantity, to be called the "normalized residuals", measures the degree to which a solution satisfies the model constraints. The normalized residual of each equation is defined as the equation imbalance divided by the largest individual term in the equation. For tracer conservation equations, the residual is the sum of the fluxes entering a volume divided by the largest of these fluxes. Small normalized residuals (<0.1, or 10%) are taken as an indication that model equations are acceptably satisfied. A solution is deemed acceptable only if all the normalized residuals associated with the model equations are 10% or less, that is, if the physical constraints are satisfied at least to the first order.

The solution which minimizes the objective function is a trade-off between model and observational constraints. If too much weight is put on the model constraints ($\mathbf{C}_f^{-1}$ too large), the observational constraints are not satisfied and vice versa. Small equation residuals are achieved by adjusting the weight matrix $\mathbf{C}_f^{-1}$ in the objective function and keeping $\mathbf{C}_0^{-1}$ constant.

The objective function J is minimized using a variant of the Gauss-Newton method [*Gill et al.*, 1981]. The method usually converges toward a local minimum of the true objective function, but if it does not, one may have to try different starting points. The procedure is considered to have converged when there is little or no progress made at each step:

$$\left\| \frac{\mathbf{x}_{k+1}}{\mathbf{x}_k} \right\| \leq 1 \pm \varepsilon \qquad (3)$$

where $\mathbf{x}_k$ and $\mathbf{x}_{k+1}$ are the estimates of the state vector at iteration k and $k+1$. The tolerance ε is a small number. At convergence, $\mathbf{f}(\mathbf{x})$ is not exactly equal to zero but should have a residual consistent with $\mathbf{C}_f$.

Because the covariance matrices $\mathbf{C}_0$ and $\mathbf{C}_f$ are diagonal, sparse matrix algorithms greatly reduce the computational load. For the model used here, a sparse matrix algorithm [*Mathworks, Inc.*, 1992] reduces the calculation time from several hours to 10 min. on a Sun Sparc 2 workstation.

3.2. The Modern-Reference Estimate: Circulation in the Present North Atlantic

The model is first used to make an estimate of the circulation of the modern deep North Atlantic, both as a test of the model structure and to provide a reference case against which to compare the LGM circulation. Potential temperature, salinity, and phosphate data are subsampled from the *Fukumori et al.* [1991] atlas every 10° in the horizontal and every kilometer in the vertical. Prior estimates of volume flux variables are computed from the thermal wind relations, using potential temperature and salinity fields and a reference level at 3 km depth or the bottom of the ocean, whichever is shallower. In the DWBC, the prior estimate of the volume flux is chosen so that the vertically integrated transport below 1 km depth is about 15 Sv. Because a small shift in the reference velocity can result in a large change in the integrated transports, we put a comparatively large, 5 Sv, error bar on this prior estimate.

Uncertainties for the prior estimates of the tracer variables are obtained from the standard deviation estimates in the *Fukumori et al.* [1991] atlas. Those values are interpolated to make them correspond to the standard depths of the model. $\mathbf{C}_0$ is assumed to be diagonal; nondiagonal matrices, implying that data misfits are correlated with their immediate neighbors, were tried as well, but they had little effect on the results, presumably because the correlations used over the horizontal grid scale (10° x 10°) are small. The diagonal elements of the weight matrix $\mathbf{C}_f^{-1}$ are determined by trial and error to obtain small equation residuals.

As shown in Figure 3, the optimization method reduced the objective function from 3×10^9 to about 10^3. After 10 iterations, no further progress was made, and the optimization procedure was stopped. The normalized equation residuals are then all below 10% (Figure 4). Mass is nearly exactly conserved with residuals smaller than 0.01%, (a consequence of the weights used), and the mean of the other normalized residuals is about 1%.

Integrated imbalances represent artificial sources of mass and tracer, but they are very small here. As indicated in Table 1, tracer imbalances integrated over the whole model domain would take about 4 million years to change the basin mean potential temperature by 1°C, 2 million years to change the mean salinity by 1, and 0.6 million years to change the mean phosphate concentration by 1 μmol/kg. There are small sources and sinks of tracers in each box, but they nearly cancel on the larger scales.

A section along 20°W (Figure 5) depicts typical changes in potential temperature, salinity, and phosphate made by the optimization. NADW remains visible in the salinity profile as the water approximately bounded by the upper and the lower 34.9 isolines (the contours are distorted compared to what one would see in the original sections from the *Fukumori et al.* [1991] atlas because of the very low resolution used here). The isolines after optimization do not depart much from the prior estimates. The biggest differences are in the phosphate section, but the optimized profiles are plausible, and the graphic differences are largely due to slight contouring shifts. All concentrations are consistent with their prior values within the estimated observational uncertainty, and a histogram of the data misfit (Figure 6) shows that most of the optimized tracer concentrations are less than one standard deviation distant from the prior value. Less than 1% of the data are more than three standard deviations from their initial values, consistent with a normal distribution.

The circulation estimated by the model (Figure 7) is a reasonable representation of normal understanding of the present circulation. We will not examine the results in detail but merely point out a few specific features to provide a sense of the compatibility between the model-inferred flow and previous descriptions. Uncertainties in the transports are calculated assuming that the weight matrix $\mathbf{C}_f$ is a reasonable approximation to the true covariance matrix of the model error.

The DWBC carries about 15 ± 2 Sv, divided into roughly equal transports of 5 Sv ± 1 Sv each in the three deepest layers of the model. The interior circulation between 1 and 2 km depths is qualitatively consistent with the circulation at 2000 dB estimated by *Martel and Wunsch* [1993] using the same *Fukumori et al.* [1991] hydrographic fields but at 1 degree resolution (compare Figure 7a with their Figure 13). The zonally integrated transport at 30°N is about 16 ± 2 Sv flow-

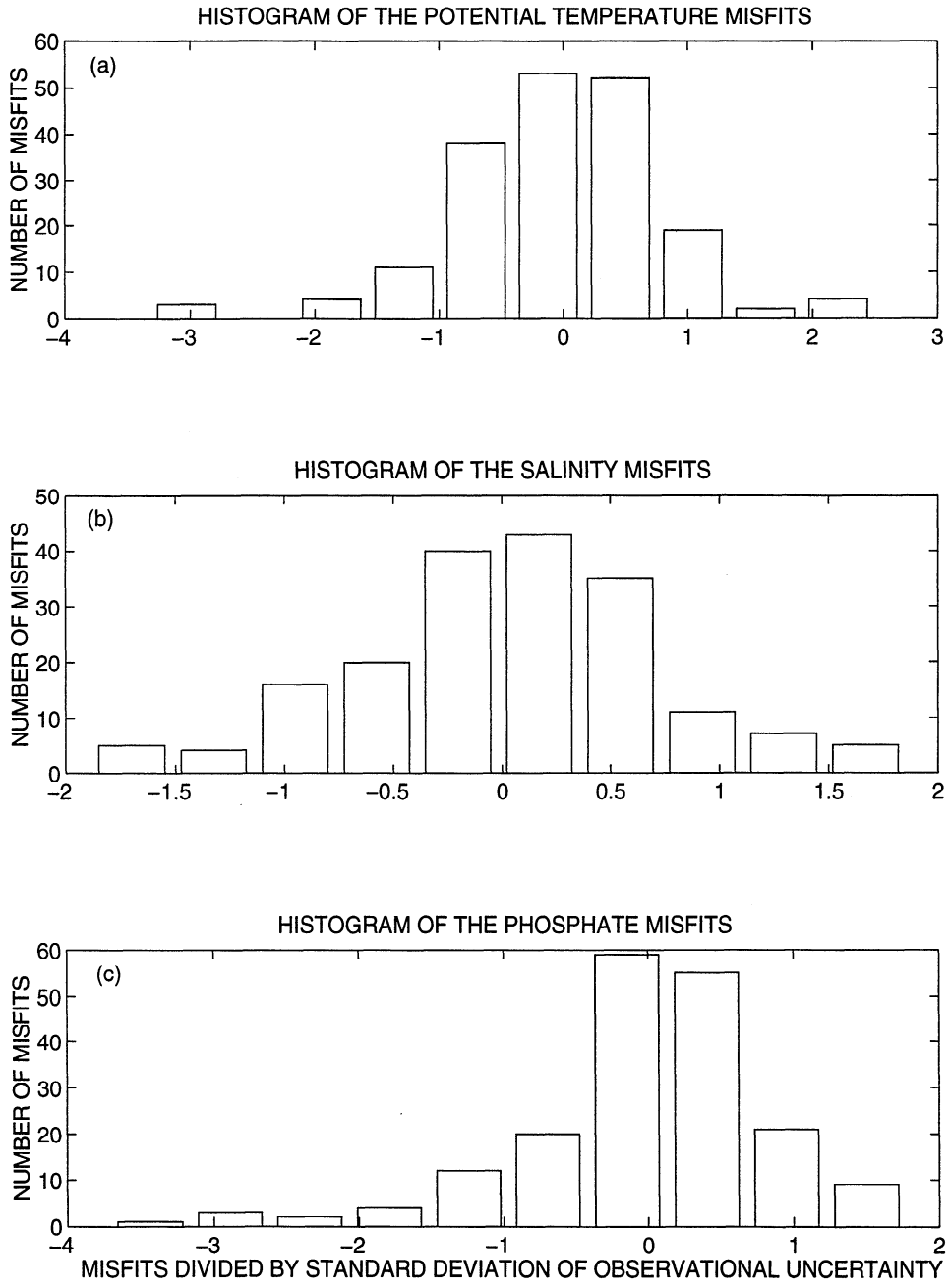

Figure 6. Histogram of the data misfits after minimization for potential temperature, salinity, and phosphate in the modern ocean run. Data misfits are defined as the tracer values estimated by the model minus the tracer values prior to inversion. The abscissa represents the data misfits divided by the standard deviation of the uncertainty in the prior estimate of the tracer value, and the ordinate represents the number of data points in each interval of the histogram. Most of the data misfits are smaller than the standard deviation of the observational uncertainty.

ing southward, which is consistent with the estimate of *Roemmich and Wunsch* [1985] from the original hydrographic sections at full resolution. There is a Mediterranean outflow of 1.6 ± 0.4 Sv between 1 and 2 km depth. This value is slightly smaller than the *Ochoa and Bray* [1991] estimate of 2.1 ± 0.3 Sv (1 Sv of outflow + 1 Sv of entrainment), but with the present coarse resolution, the difference is acceptable. Water originating in the Mediterranean outflow spreads southwestward to sustain the Mediterranean salt tongue, which is the most noticeable feature in the data at intermediate depths.

The flow is northward in the deepest level of the eastern Atlantic (between 4 km and 5 km depth; Figure 7d). *McCartney et al.* [1991] calculated that there are about 4 Sv moving northward as an eastern boundary current along the Mid-

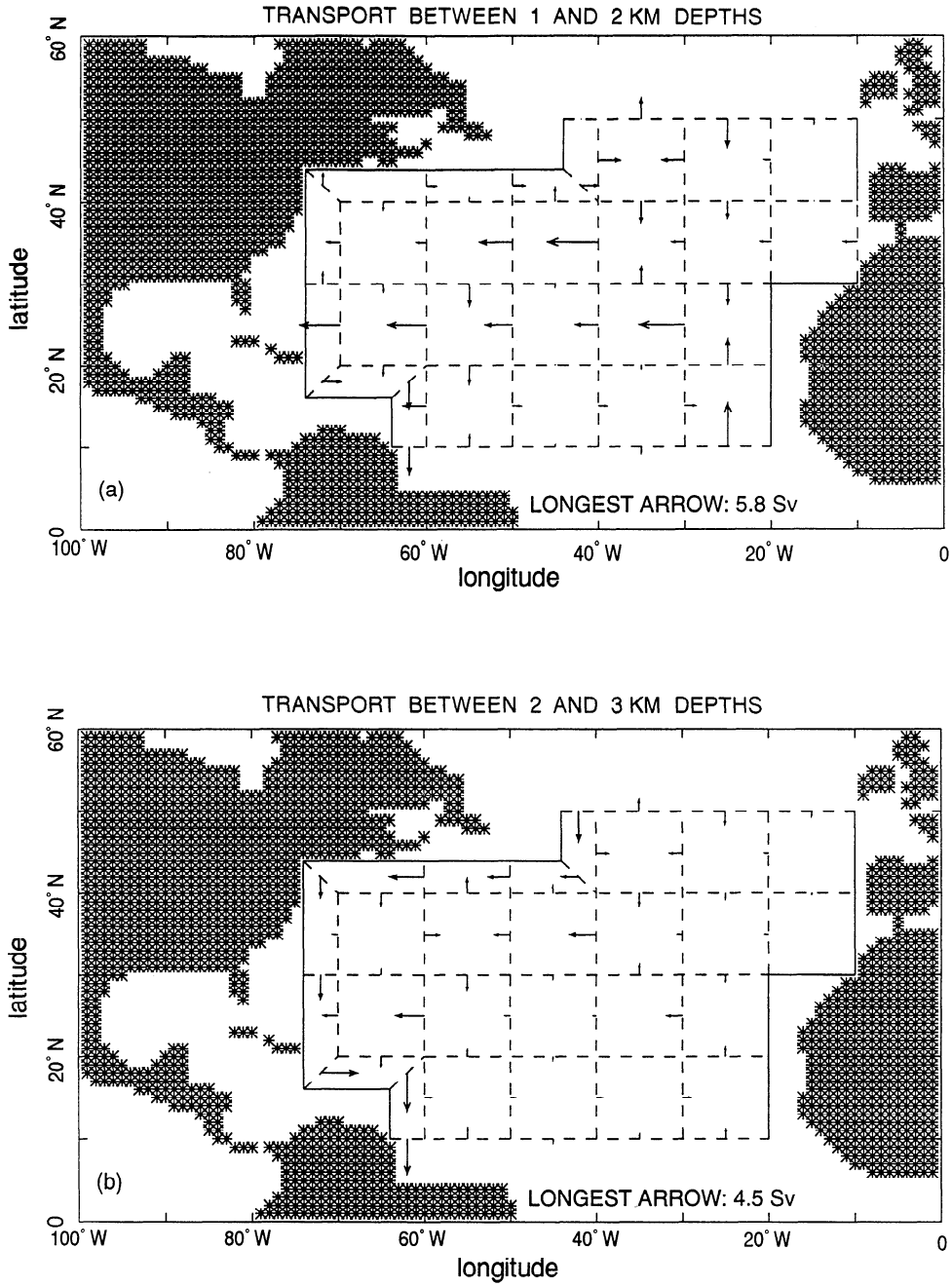

Figure 7. Horizontal transports (in Sverdrups) in the different layers of the model, estimated for the modern ocean. The transport associated with the longest arrow is indicated below each panel. Vectors in the westernmost boxes represent the transports in the DWBC.

Atlantic Ridge, becoming 2 Sv northward in the eastern Atlantic, north of the Vema fracture zone at 10°N. Below 4 km depth, the model estimates 0.65 ± 0.1 Sv moving northward between the American continent and the Mid-Atlantic Ridge and 1 ± 0.1 Sv northward between the Mid-Atlantic Ridge and the African coast. In the absence of uncertainty estimates for the *McCartney et al.* [1991] results and because of the poor temporal sampling available for the ocean, there is no reason to regard the model-inferred flow as unrealistic. The northward and southward zonally integrated transports (sum of all the northward transports and sum of all the southward transports across a given section) indicate a maximum southward transport across 10°N located between 3 and 4 km depths (Figure 8), consistent with the expected southward spreading of NADW.

We have thus produced an estimated solution which is consistent with the available modern hydrographic data and simplified, yet realistic physics and which is quantitatively ac-

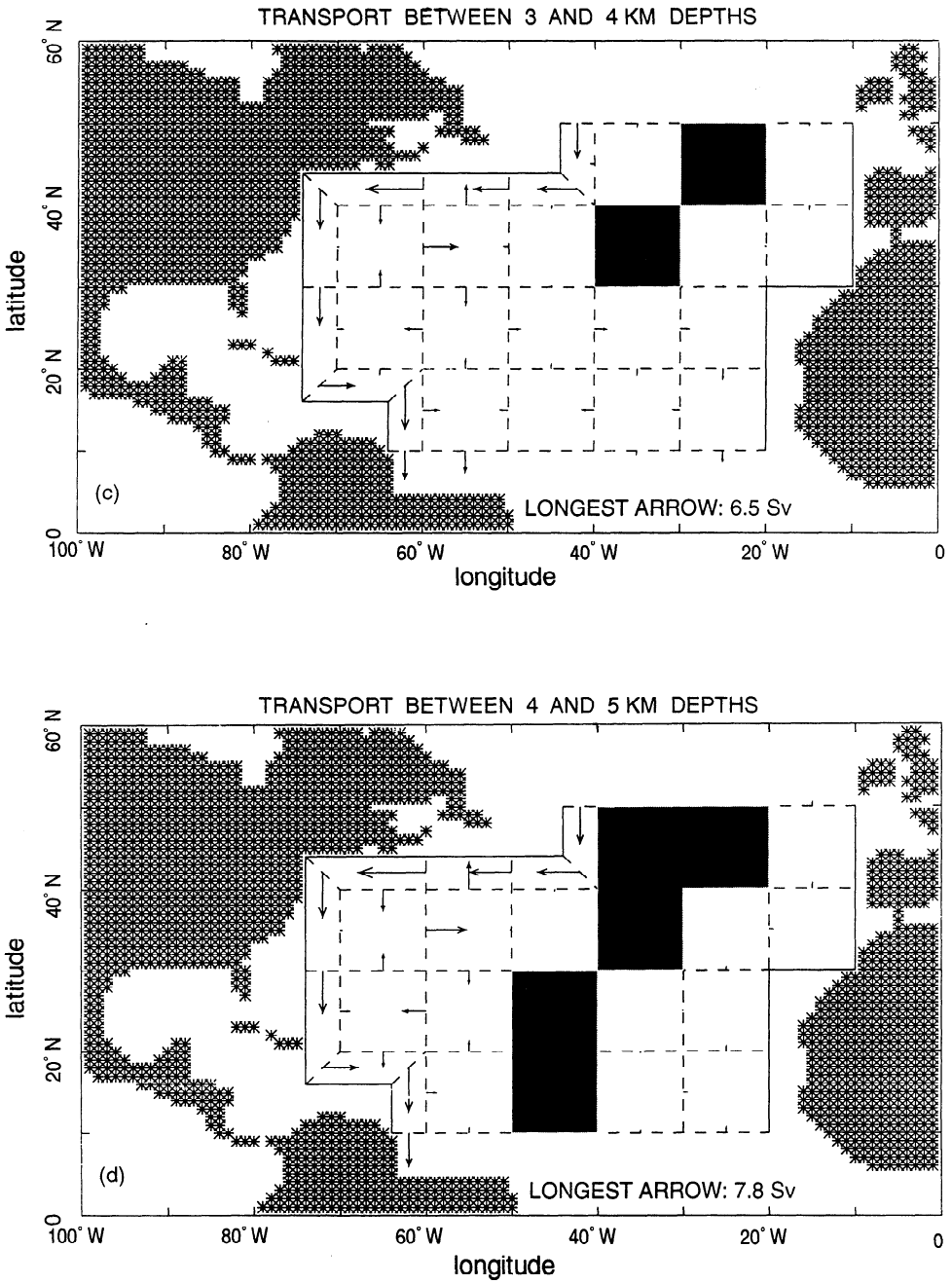

Figure 7. (continued)

ceptable. These results will be used as a self-consistent reference flow to be compared with similar calculations from the LGM ocean.

3.3. Last Glacial Maximum Inversions

The same inverse model as the one used to estimate the modern ocean circulation can be applied to explore the range of circulations consistent with paleoclimate data. The model is constrained with $\delta^{13}C$ and $\delta^{18}O$ data that we compiled from published records but also from a few unpublished data obtained from personal communications. This compilation is listed in Table 2. Most data points are given by *Sarnthein et al.* [1994]. All the data come from measurements made on the benthic foraminifera Cibicidoides. This genus is thought to most reliably record the $\delta^{13}C$ of total inorganic carbon dissolved in the deep ocean as well as the $\delta^{18}O$ of seawater (with an offset due to temperature effects and a constant offset of 0.64 ‰ due to vital effects [see *Mix*, 1987]; the 0.64 ‰ offset is taken into account in the data set). In the compilation, both $\delta^{13}C$ and $\delta^{18}O$ are referenced to the Pee Dee belemnite (PDB) standard. An intercalibration problem exists between the different laboratories measuring $\delta^{18}O$ and can create an offset of more than 0.1 ‰ between different data sets [*Zahn and Mix*, 1991]. No systematic interlaboratory calibration has been carried out, and it is not clear how best to account for the discrep-

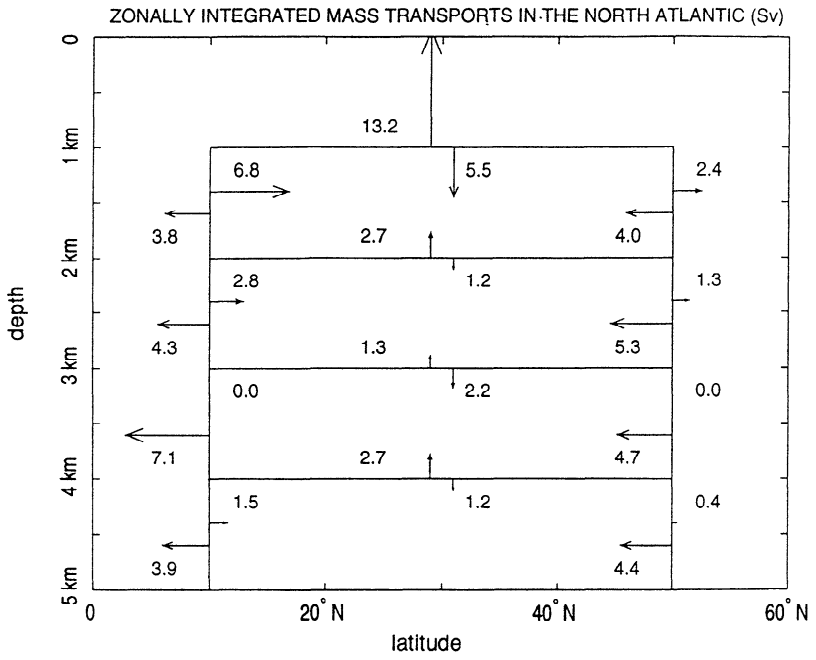

Figure 8. Zonally integrated mass transports in the North Atlantic (in Sverdrups) estimated for the modern ocean. Northward and southward integrated transports are the sum of all the northward going transports and the sum of all the southward going transports. The slight imbalance in the upper layer is compensated by the inflow from the Mediterranean.

ancy. Here the $\delta^{18}O$ data are entered in the compilation with no correction, and possible bias errors are included in the estimate of the observational uncertainties.

There are about 100 $\delta^{18}O$ and $\delta^{13}C$ data points for the LGM in the North Atlantic (Figure 2) mostly from the eastern basin and less than 30 data points in the South Atlantic. For some sediment cores, only one of $\delta^{18}O$ or $\delta^{13}C$ values is published.

3.3.1. Treatment of $\delta^{13}C$ and $\delta^{18}O$ in the LGM runs. In the model, $\delta^{18}O$ data are converted to temperature variables through the relation:

$$T = -4.0\,(\delta^{18}O_c - \delta^{18}O_w) + 16.9 \qquad (4)$$

([*Shackleton*, 1974] T in Celsius; relation valid for T<16°C). Here $\delta^{18}O_c$ is the $\delta^{18}O$ value measured in foraminifera shells, and $\delta^{18}O_w$ is the $\delta^{18}O$ of seawater. Both $\delta^{18}O_c$ and $\delta^{18}O_w$ are expressed in per mil and must be referenced to the same standard.

The contribution of the unknown $\delta^{18}O_w$ term to temperature vanishes in the potential temperature conservation equation when mass is conserved because $\delta^{18}O_w$ is a conservative property. It does contribute to the thermal wind equations, however, because the gradients of $\delta^{18}O_w$ appear in the expression for the density gradients:

$$\nabla_h \rho = \alpha \times \nabla_h T + \beta \times \nabla_h S$$
$$= -4.0 \times \alpha \times \nabla_h (\delta^{18}O_c - \delta^{18}O_w) + \beta \times \nabla_h S \qquad (5)$$

where ∇_h denotes the horizontal gradient operator and α and β are the coefficients of the linear equation of state. The gradients of density cannot be computed from the paleodata because $\nabla_h\,\delta^{18}O_w$ is unknown, and thus, unlike the modern ocean problem, the thermal wind balance only weakly constrains the circulation. Here, as a best case, it is assumed that $\nabla_h\,\delta^{18}O_w = 0$. This assumption is not realistic because $\nabla_h\,\delta^{18}O_w$ is of comparable magnitude to $\nabla_h\,\delta^{18}O_c$, albeit smaller. Even with this approximation, density gradients remain unknown because salinity cannot be estimated. In the absence of observational constraints on paleosalinities, salt conservation is required and the salinity gradients are to be minimized (salinity almost homogeneous). The two assumptions, $\nabla_h\,\delta^{18}O_w = 0$ and $\nabla_h S \approx 0$, are not justified but do permit exploration of the hypothesis that the density is controlled by temperature alone. As shown below, there are at least two ocean circulations consistent with the paleodata and which satisfy these drastic assumptions. If the assumptions are not made, the paleocirculation is even less constrained and an even wider set of circulations than we will find would be acceptable.

No phosphate data exist for the LGM ocean, and $\delta^{13}C$ data are used instead. Different apparent water masses are visible in the modern meridional section of $\delta^{13}C$ (Figure 1a), and like phosphate, $\delta^{13}C$ can be considered in first approximation as an almost conservative tracer in the North Atlantic. In the absence of biological activity, conservation equations for ^{13}C and ^{12}C can be written in each box as

$$\Sigma_i U_i \times {}^{13}C_i = \Sigma_i U_i\,(1 + \delta^{13}C_i / 1000) \times {}^{12}C_i \approx 0 \qquad (6)$$

$$\Sigma_i U_i \times {}^{12}C_i \approx 0 \qquad (7)$$

Subtracting (7) from (6) and multiplying by 1000, one obtains

$$\Sigma_i U_i \times {}^{12}C_i \times \delta^{13}C_i \approx 0 \qquad (8)$$

Table 2. Data Compilation for the Last Ice Age, Obtained From Measurements in Foraminifera Shells

Core	Lat °N	Long °E	Depth, m	$\delta^{13}C$ ‰	$\delta^{18}O$ ‰	$\delta^{13}C_m$ ‰	$\delta^{13}C$	$\delta^{18}O$	$\delta^{13}C_m$
M16004	29.98	-10.65	1512	1.16	4.58	1.12	Sar94	Zah91	Sar88
M16006	29.25	-11.50	796	1.50	4.02	1.17	Sar88	Zah91	Sar88
M15627	29.17	-12.09	1024	1.45	4.15		Sar94	Zah91	
M15637	27.01	-18.99	3849	0.38	4.99	0.92	Sar88	Zah91	Sar88
M12309	26.84	-15.11	2820	0.29	4.99	0.99	Sar88	Zah91	Sar88
M12392	25.17	-16.85	2575	0.36	5.15	0.97	Dup88	Dup88	Sar88
M12310	23.50	-18.72	3080	0.35		1.06	Sar94		Sar94
M12379	23.14	-17.75	2576	0.47	5.07	0.93	Sar88	Zah91	Sar88
M16017	21.25	-17.80	812	1.13	3.88	0.99	Sar94	Zah91	Sar94
M16030	21.24	-18.06	1516	0.89	4.83	0.88	Sar88	Zah91	Sar88
M12328	21.15	-18.57	2778	0.23	5.01	0.82	Sar94	Zah91	Sar88
M12329	19.37	-19.93	3320	0.20		0.85	Sar94		Sar94
M13289	18.07	-18.01	2490	0.42	5.00	0.98	Sar88	Zah91	Sar88
M12337	15.95	-18.13	3088	-0.10		0.67	Sar94		Sar94
M12347	15.83	-17.86	2576	0.35	5.10	0.88	Sar88	Sar88	Sar88
M12345	15.48	-17.36	945	0.97	4.28	0.75	Sar94	Zah91	Sar94
M16402_2	14.46	-20.54	4234	-0.18	5.24	0.60	Sar88	Sar88	Sar88
M16415	9.57	-19.11	3841	0.27	5.24	0.69	Sar88	Sar88	Sar88
M16407	9.04	-21.96	4596	0.03		0.75	Sar94		Sar94
M16408	9.01	-21.37	4336	-0.04	4.94	0.59	Sar88	Sar88	Sar94
M16459	7.27	-26.20	4785	-0.13			Sar94		
M17049	55.15	-26.44	3331	0.47		0.63	Sar94		Sar94
M17055	48.22	-27.06	2558	0.94		1.24	Sar94		Sar94
M15612_2	44.69	-26.54	3050	0.62	5.14	1.10	Sar94	Zah91	Sar88
M17048	54.31	-18.18	1859	1.23		1.31	Sar94		Sar94
M17045	52.43	-16.66	3663	0.26		0.79	Sar94		Sar94
M11944	35.65	-8.06	1765	1.00	4.65	1.21	Sar88	Zah91	Sar88
M15666	34.96	-7.12	803	1.58	3.69	1.34	Sar94	Zah91	Sar94
M15670	34.91	-7.58	1482	1.32	4.50	1.08	Sar94	Zah91	Sar88
M15669_1	34.89	-7.82	2022	0.81	4.99	1.15	Sar94	Zah91	Sar88
M15672	34.86	-8.12	2455	0.68	5.11	1.22	Sar94	Zah91	Sar88
M13519	5.66	-19.85	2862	0.37	5.25	0.99	Dup88	Dup88	Sar88
M16457	5.39	-21.72	3291	0.11	4.64	1.00	Sar88	Sar88	Sar88
M16458	5.34	-22.06	3518	-0.02	4.94	0.80	Sar88	Sar88	Sar88
M16455	5.27	-22.87	4610	-0.05		0.65	Sar94		Sar94
M16453_2	4.73	-20.95	2675	0.47	5.14	1.01	Sar88	Sar88	Sar88
M13521_1	3.02	-22.03	4504	-0.42	5.00	0.82	Sar88	Sar88	Sar88
M13239	13.88	-18.31	3156	0.08	5.19	0.86	Sar88	Zah91	Sar88
V23_100	21.30	-22.68	4579	0.0		0.59	Dup88		Sar88
V22_197	14.17	-18.58	3167	0.17	5.00	0.76	Dup88	Dup88	Sar88
V22_196	13.83	-18.97	3728	-0.20	5.14	0.85	Dup88	Dup88	Sar88
V29_179	44.00	-24.53	3331	0.63	5.23	1.10	Sar94	Zah91	Sar88
V25_59	1.37	-33.48	3824	0.07	4.95	0.89	Dup88	Dup88	Sar88
V30_40	-0.20	-23.15	3706	-0.11	4.53		Dup88	Dup88	
V23_81	54.25	-16.83	2393	0.61		0.93	Sar94		Sar94
V30_49	18.45	-21.08	3093	0.21	5.03	0.91	Dup88	Dup88	Cur88
V26_176	36	-72	3942	0.18	4.69	0.87	Cur88	Cur88	Cur88
V28_127	12	-80	3623	1.2	4.54		Opp90	Opp90	
V28_14	64.78	-29.57	1855	1.21	4.96	0.80	Cur88	Cur88	Cur88
V22_188	4.67	-20.92	2600	0.74	4.80		Dup88	Dup88	
V29_144	0.20	6.05	2685		4.85			Zah91	
V26_46	9.57	-18.18	2898		4.77			Zah91	
V32_08	34.78	-32.42	3252		4.98			Zah91	
V29_177	41.53	-25.72	3391		5.04			Zah91	
V30_51K	19.87	-19.92	3409		4.84			Zah91	
V29_178	42.85	-25.15	3448		4.80			Zah91	
V30_239	23.57	-20.07	3901		5.12			Zah91	
V30_36	5.35	-27.32	4245		5.01			Zah91	
V30_97	41.00	-32.93	3371		5.2			Rud84	
EN066_16	5.46	-21.14	3152	0.45	4.83	0.83	Cur88	Cur88	Cur88
EN066_10	6.65	-21.90	3527	0.33	4.65	0.82	Cur88	Cur88	Cur88
EN066_44	5.26	-21.71	3428	0.50	4.99	1.04	Cur88	Cur88	Cur88
EN066_38	4.92	-20.50	2931	0.51	4.61	1.14	Cur88	Cur88	Cur88
EN066_21	4.23	-20.62	3995	0.24	4.56	0.80	Cur88	Cur88	Cur88

Table 2. (continued)

Core	Lat °N	Long °E	Depth, m	$\delta^{13}C$ ‰	$\delta^{18}O$ ‰	$\delta^{13}C_m$ ‰	$\delta^{13}C$	$\delta^{18}O$	$\delta^{13}C_m$
EN066_26	3.09	-20.02	4745	-0.07	4.76	0.84	Cur88	Cur88	Cur88
EN066_32	2.47	-19.73	5003	-0.25	4.73	0.89	Cur88	Cur88	Cur88
EN066_29	2.46	-19.76	5104	-0.19	4.39	0.85	Cur88	Cur88	Cur88
EN066_36	4.31	-20.21	4270	0.11	4.87	0.69	Cur88	Cur88	Cur88
CHN825020	43.50	-29.87	3020	0.70	5.00	1.25	Dup88	Dup88	Sar88
CHN82_11	42.00	-32.00	3209	0.66	5.02		Dup88	Dup88	
CH73_139	54.63	-16.35	2209	0.62	5.18	0.93	Cur88	Cur88	Cur88
CH72_02	40.60	-21.70	3485	0.77	4.91	0.90	Dup88	Dup88	Cur88
CH71_07	4.38	-20.87	3083	0.30	5.16	1.08	Dup88	Dup88	Sar88
CH82_24_4	41.72	-32.85	3427	0.53	4.73	1.02	Cur88	Cur88	Cur88
CH74_227	35.25	-29.25	3225	0.18	5.08	0.46	Dup88	Dup88	Cur88
CH75_03	10.05	-57.53	3410	0.13	5.31	0.87	Dup88	Dup88	Cur88
CH75_04	10.05	-56.05	3820	-0.21	5.22	0.67	Dup88	Dup88	Cur88
CH74_23_1	36.87	-26.62	2354	0.56	4.89	1.00	Dup88	Dup88	Sar88
KNR110_66	4.56	-43.38	3547	0.19	4.36	0.71	Cur88	Cur88	Cur88
KNR110_91	4.76	-43.31	3810	0.08	4.45	0.71	Cur88	Cur88	Cur88
KNR110_50	4.86	-43.20	3995	0.20	4.66	0.65	Cur88	Cur88	Cur88
KNR110_58	4.79	-43.34	4341	-0.03	4.73	0.62	Cur88	Cur88	Cur88
KNR110_55	4.95	-42.89	4556	-0.01	4.61	0.40	Cur88	Cur88	Cur88
KNR110_82	4.34	-43.49	2816	0.21	4.71	1.11	Cur88	Cur88	Cur88
KNR110_75	4.34	-43.41	3063	0.28	4.38	0.97	Cur88	Cur88	Cur88
KNR110_71	4.36	-43.70	3164	0.40	4.50	1.10	Cur88	Cur88	Cur88
KNR64_5_5	16.52	-74.81	3047	1.25	3.94	0.95	Sar88	Sar88	Sar88
NA87_22	55.50	-14.70	2161	0.70		1.08	Sar94		Sar94
SU81_44	44.25	-2.70	1173	1.06	4.74		Sar94	Zah91	
KS_11	40.69	-10.21	3590	0.63			Sar94		
SU81_21	38.25	-9.55	1260	0.98	4.34		Sar94	Zah91	
SU81_18	37.77	-10.18	3135	0.11		0.77	Sar94		Sar94
LYII_13A	35.97	-7.82	1201	1.58	4.06		Sar94	Zah91	
T86_15	30.26	-37.04	3375	0.53		1.15	Sar94		Sar94
KW_31	3.18	5.57	1181	0.60	4.58	0.29	Dup88	Dup88	Sar94
NO75_08	45.7	-31.37	3454	0.59	5.12	1.07	Dup88	Dup88	Sar88
S58_798	42.83	-23.07	3520	0.60	4.92	0.92	Dup88	Dup88	Sar88
K708_7	54.93	-24.08	3502		4.5			Rud84	
DSDP552	56.05	-23.22	2311	0.94	4.73	1.29	Sar88	Zah91	Sar88
SU81_45	44.10	-2.48	994	1.10	4.51		Dup88	Dup88	
ODP658	20.75	-18.58	2263	0.49	5.14	0.80	Sar88	Sar88	Sar88
ODP659	18.08	-21.03	3069	0.16		0.99	Sar94		Sar94
ALB_226	17.95	-21.05	3100	0.04		0.88	Sar94		Sar94
IOS82	42.38	-23.52	3540	0.44			Boy92		
DSDP606	37.34	-35.5	3007	0.45	4.8		Kei	Kei	
V22_174	-10.07	-12.82	2630	0.72	4.77	0.80	Dup88	Dup88	Sar88
V19_240	-30.58	-13.28	3103	0.02	4.99		Dup88	Dup88	
CIR_211	-20.00	10.75	1300	0.28	4.30	0.24	Dup88	Dup88	Sar94
RC13_229	-25.50	11.33	4191	-0.41	4.90	0.33	Dup88	Dup88	Cur88
RC13_228	-20.33	11.20	3204	-0.10	5.05	0.49	Dup88	Dup88	Cur88
RC12_294	-37.27	-10.06	3308	-0.23	4.83	0.81	Dup88	Dup88	Sar88
RC15_94	-42.98	-20.85	3762	-0.52	5.03		Dup88	Dup88	
CHN115_92	-30.43	-38.83	3934	-0.43	4.68	0.13	Dup88	Dup88	Sar88
CHN115_70	-29.92	-35.65	2340	0.71		0.95	Sar88		Sar88
CHN115_91	-30.80	-38.43	3576	0.23		0.62	Sar88		Sar88
CHN115_88	-30.92	-36.08	2941	0.34		0.68	Sar88		Sar88
AII60_13A	-31.98	-36.65	2739	0.43		1.17	Sar88		Sar88
INMD_113	-15.25	-14.97	3471	0.47		0.94	Sar88		Sar88
INMD_115	-17.67	-16.22	3427	0.48		0.92	Sar88		Sar88
M16772	-1.21	-11.96	3912	-0.18		0.86	Sar94		Sar94
M16867	-2.20	5.10	3891	-0.22		0.81	Sar94		Sar94
BT4	-4.33	10.43	1000	0.24		0.38	Sar94		Cur88
MG_237	-5.20	11.33	1000	-0.10		-0.11	Sar94		Sar94
M1113_4	-5.75	-11.04	2374	0.45		0.93	Sar94		Sar94
RC11_83	-41.30	14.48	4718	-0.67			Sar94		

Measurements from foraminifera shells are *Cibicidoides* species only; the $\delta^{18}O$ values are referenced to the *Uvigerina* species. Columns 1 to 4 give the name, latitude, longitude, and depth of the core; columns 5 and 6 give last glacial maximum (LGM) $\delta^{13}C$ and $\delta^{18}O$ values in per mil; column 7 gives core top $\delta^{13}C$ values in per mil; columns 8 to 10 give the sources of the LGM $\delta^{13}C$, LGM $\delta^{18}O$, and core top $\delta^{13}C$ data. References are Cur88, *Curry et al.* [1988]; Sar88, Sarthein et al. [1988]; Dup88, *Duplessy et al.* [1988]; Zah91, *Zahn and Mix* [1991]; Sar94, *Sarthein et al.* [1994]; Opp90, *Oppo and Fairbanks* [1990]; Rud84, *Ruddiman and McIntyre* [1984]; Boy92, *Boyle* [1992]; Kei, *L. Keigwin* (personal communication, 1993).

Typically, ^{12}C = O(2000) ± 50 μmol/kg, at least locally. In the model, we assume that it is a constant over each box so carbon 13 conservation equations can be rewritten as

$$\Sigma_i U_i \times \delta^{13}C_i \approx 0 \quad (9)$$

Accounting for the effect of ^{12}C variations, as well as biological particle fluxes, results in a larger number of poorly known parameters and further reduces the capability of paleodata to constrain the oceanic circulation. Thus, here again, the assumptions made correspond to a best-case situation, and one expects a larger range of possible solutions in more elaborate models.

3.3.2. Observational uncertainty in the paleodata. The analytical precision of $\delta^{13}C$ measurements is about 0.05 ‰, and that of $\delta^{18}O$ is better than 0.1 ‰ (E. Boyle, personal communication, 1993). However, there are other sources of uncertainty such as bioturbation which are larger than the analytical precision. Bioturbation is the mixing of the upper 10 cm, or so, of the sediments by fauna living there. Because the average sedimentation rate of the world ocean is 2 to 5 cm per thousand years [*Broecker and Peng*, 1982], bioturbation limits the time resolution of most sediment cores to a few thousand years. It smoothes out the extrema of $\delta^{18}O$ and $\delta^{13}C$ values and introduces some error in the LGM data. Quantifying this error is difficult because it requires information about sedimentation rates and models of the effects of mixing on the tracer records. For this reason, most observations are published without estimates of the observational uncertainties.

Yet another source of error in $\delta^{13}C$ records arises from the fallout of organic matter onto the sediments in high-productivity regions. Organic matter is depleted in $\delta^{13}C$, and because a significant fraction of it dissolves at the sediment-water interface, it tends to lower the $\delta^{13}C$ of the bottom water in which foraminifera grow. In this case, the $\delta^{13}C$ recorded in foraminifera shells does not reflect the composition of the overlying water mass. Instead, it is representative of the water a few millimeters above the sediment-water interface [*Mackensen et al.*, 1993]. It is difficult to quantify this offset between the foraminifera and the water mass composition. In low productivity regions, essentially all the organic matter dissolves in the upper and intermediate layers of the ocean and does not influence the benthic $\delta^{13}C$ record. Thus the error introduced by fallout of organic matter is probably significant only in high-productivity regions. Generally speaking, cores located below mid-latitude gyres are more likely to be affected by bioturbation because of the low sedimentation rates there; cores located near polar fronts in the Southern Ocean and cores from the upwelling regions off the African coast are more likely to be affected by fallout of organic matter.

Finally, because the location of the sediment cores used in the compilation does not correspond to model grid points, it is necessary to interpolate or extrapolate the data to the grid. This mapping was done subjectively. In general, the closest data points were attributed to each model grid point, except in cases where there were discrepancies between close data points. In this case, the most plausible neighboring value was chosen. This subjective mapping results in some additional uncertainty, especially in regions where the data are scarce.

Because individual estimates of the observational uncertainty for every published data point are not available, the precision of the observations is assumed to be the same for every data point. This assumption is unrealistic because accumulation rates and biological productivity differ from one region to another. However, *Sarnthein et al.* [1994] showed

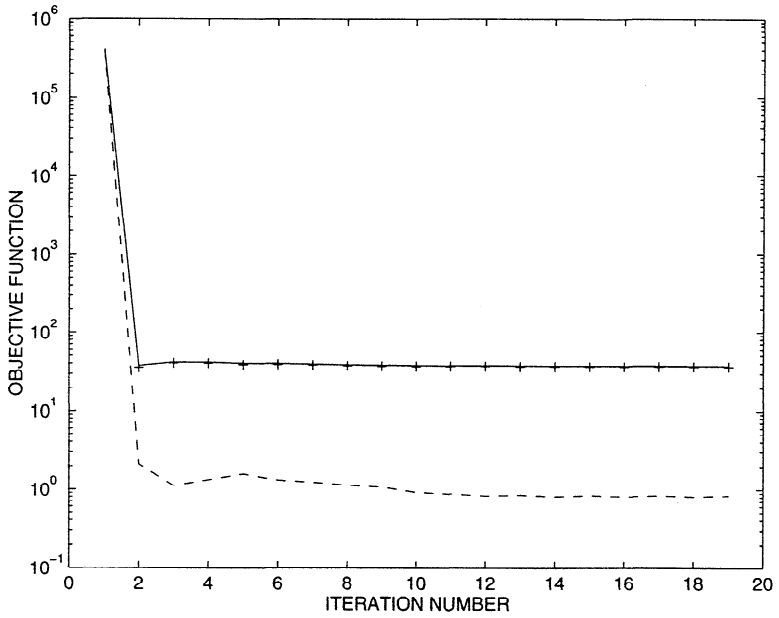

Figure 9. Objective function versus the number of iterations for the LGM run 1 (modern circulation as the prior value). Symbols are the same as in Figure 3. An infinite weight is put on the nonlinear physical constraints. These constraints are not satisfied exactly, however, because the minimization is stopped after a limited number of iterations and because of numerical round off errors. The objective function is the sum of the data misfit term and of the contribution of the linear physical constraints.

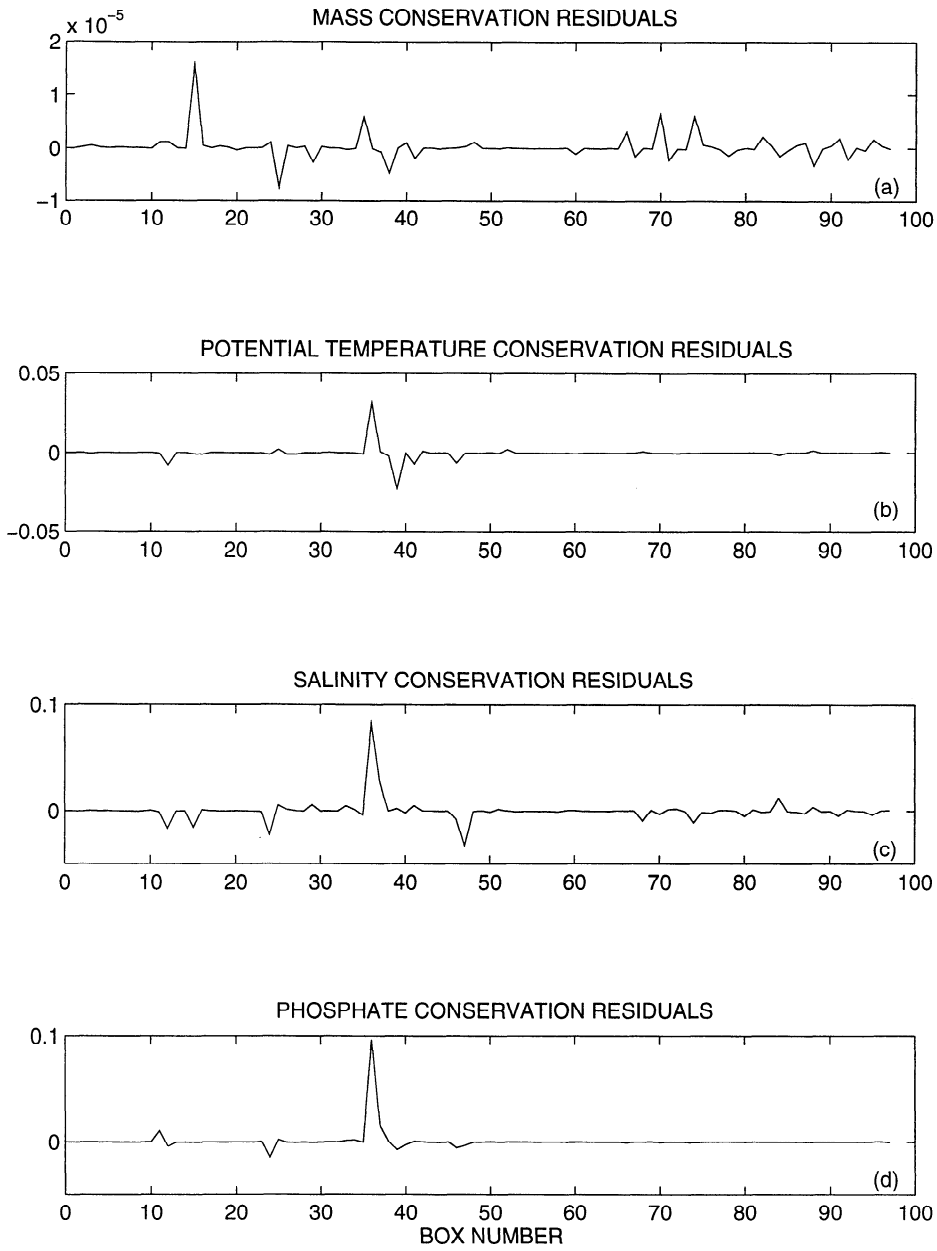

Figure 10. Residuals after minimization, as in Figure 4, but for the LGM run 1.

that, in general, $\delta^{13}C$ values recorded in sediment core top foraminifera shells deviate from $\delta^{13}C$ values of dissolved inorganic carbon measured in seawater (interpolated between nearby stations) with a standard deviation of about 0.2 ‰. The uncertainty introduced by our mapping procedure differs from the uncertainty introduced by their interpolation scheme, but we nevertheless adopt their estimate of 0.2 ‰ for the standard deviation of the $\delta^{13}C$ data uncertainty combined with the mapping uncertainty. The same standard deviation is also used for the $\delta^{18}O$ data (which is a plausible assumption in terms of the average discrepancy between nearby data points). Note that this 0.2 ‰ observational uncertainty for $\delta^{18}O_c$ translates into a 0.8°C uncertainty in the estimate of the temperature field, a large value for the deep ocean and especially so if the gradients of temperature are required, as in the thermal wind equations.

Uncertainties in the estimates of the volume transports after optimization are calculated assuming an uncertainty of 5 Sv on the transports prior to optimization. This large prior uncertainty reflects the lack of independent constraints, besides tracer data, on the LGM circulation.

3.4. Paleocirculation Estimate 1: The Modern Circulation as the Prior Value

This computation specifically addresses the important question of whether the paleotracer data require a circulation, particularly of the NADW flux, radically different from today.

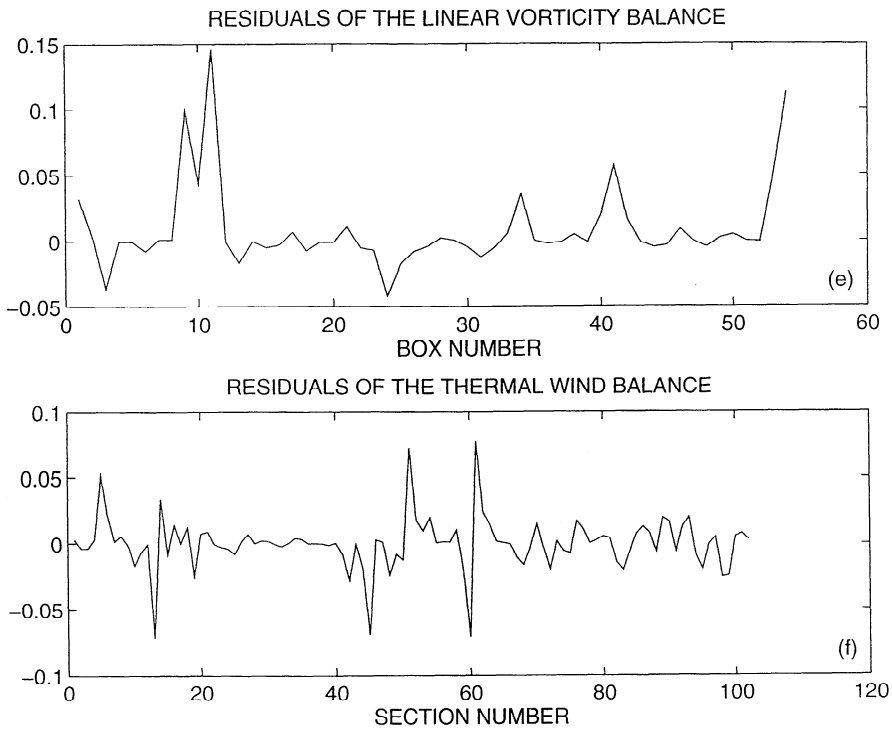

Figure 10. (continued)

The flux of NADW is represented in the model by the zonally integrated transports at 50°N. The prior estimate of the circulation is initialized by the modern ocean circulation described above, and a large weight is used in the associated term in the objective function to constrain the model to find small modifications to the prior estimate. Two sets of tracer data are employed: $\delta^{18}O$ converted to temperature and $\delta^{13}C$. The modern ocean model salinity distribution is used in the initialization as there are no LGM observations of it, but a very large uncertainty (small weight) is used. The posterior salinity field is constrained to be very smooth by adding a term to the objective function which penalizes salinity gradients. This term is proportional to $\nabla_h^2 S$ where ∇_h^2 denotes the horizontal Laplacian operator.

Where $\delta^{18}O$ and $\delta^{13}C$ data are available, an uncertainty of 0.2 ‰ is used. Where no data are available, we extrapolate and attribute the same uncertainty of 0.2 ‰ to the extrapolated $\delta^{18}O$ and $\delta^{13}C$ values. Such a small uncertainty for the extrapolated values cannot be defended rigorously, but otherwise, the model tends to produce extrema in the tracer concentrations in the interior of the model domain. These extrema are not physical but are artifacts of the numerical discretization of the tracer conservation equations.

Following optimization, the objective function is greatly reduced (Figure 9), and mass is almost perfectly conserved as required (Figure 10a). All model physical constraints are satisfied at a level of 10%, and the average deviation is about 1% (Figure 10), with imbalances integrated over the whole model domain being very small (Table 1).

The tracer field obtained after inversion is visually slightly different from the original distribution (Figure 11) but is consistent with the data within the estimated uncertainty (Figure 12). The departures from the data do not follow a normal distribution, with most of the departures close to zero and only a few misfits larger than one standard deviation (0.2 ‰). The optimized salinity field is almost homogeneous; its range of variation is about 0.02 at 20°W (Figure 11b) owing to the strong smoothness requirement imposed on the model.

The central conclusion to be drawn from this calculation is that the paleodata are consistent with the modern circulation (compare Figure 13 with Figure 7) and do not, by themselves, require an LGM circulation perceptibly different. The maximum difference between the glacial and the modern zonally integrated transports across 50°N is 0.7 Sv, in the deepest layer of the model (compare Figure 14 with Figure 8). The zonally and vertically integrated transport between 1 and 5 km depth across 30°N is 16 ± 2 Sv in the modern ocean run and 17 ± 4 Sv in the LGM estimate. It is only in some details that differences become apparent. The exchange of mass across 10°N is very similar to that of the modern ocean. Yet in the upper layer, there is slightly less water going north (Figure 14 and Figure 8). The core of NADW is shifted slightly upward: the southward transport between 2 and 3 km depths goes up from 4 ± 1 Sv in the modern ocean to 5 ± 4 Sv during the LGM, and the southward transport between 3 and 5 km depth goes from 11 ± 1 Sv in the modern ocean down to 9 ± 3 Sv during the LGM. This shift is in the direction of the conventional interpretation of the paleodata (reduction of the flux of Lower NADW), but given the uncertainty in the estimated fluxes, such small changes are not significant. In contrast too, the northward flow through 10°N in the bottom layer shifts from 1.5 ± 0.2 Sv down to 0.6 ± 2 Sv (Figures 8 and 14). This reduction of the flux of water coming from the South Atlantic suggests a reduction of the flux of AABW. Even if the circu-

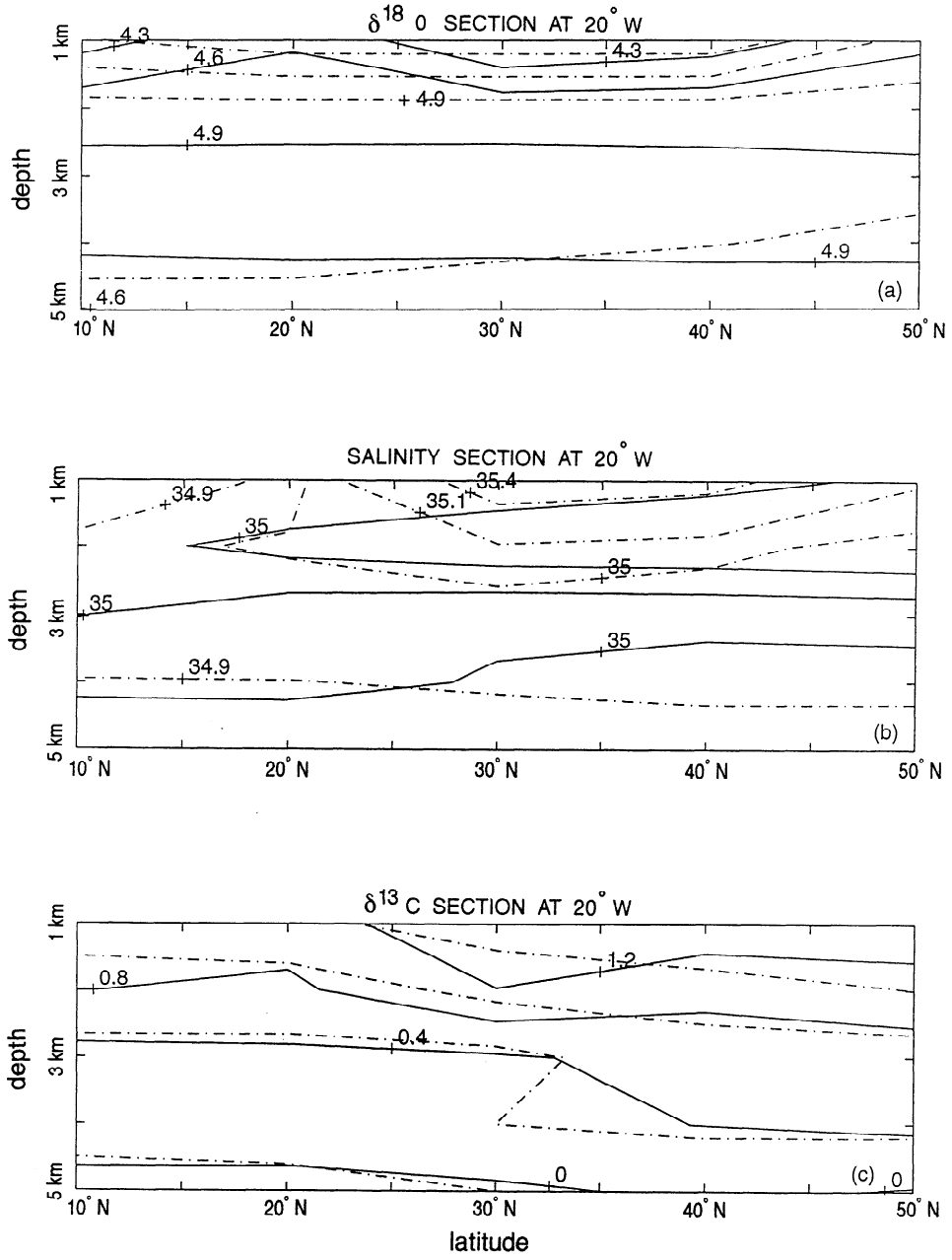

Figure 11. Meridional sections of $\delta^{18}O$ (in per mil), salinity (Practical Salinity Scale), and $\delta^{13}C$ (in per mil) obtained in the LGM run 1 at 20°W. Symbols are the same as in Figure 5. Note that the posterior salinity distribution is almost homogeneous.

lation changes were deemed to be significant, the reduction of the flux of AABW would be proportionally larger than the reduction of the flux of NADW, which would contradict the conventional interpretation of the data (which argues for a reduced flux of NADW, the flux of AABW being fixed, or more generally a reduction of the ratio of the flux of NADW over the flux of AABW [*Boyle and Keigwin*, 1982]).

Thus this calculation suggests that the modern ocean circulation is consistent with the LGM $\delta^{13}C$ and $\delta^{18}O$ data and that significant circulation changes are not required. We will discuss this important result in section 5, but we will first examine another calculation which will help understanding of the problem.

3.5. Paleocirculation Estimate 2: Lower NADW Production Reduced to Half Its Modern Value

Although we have shown that the paleodata used do not require a circulation differing significantly from the modern one, we strongly emphasize that this conclusion is very different from deducing that the LGM circulation was actually the same

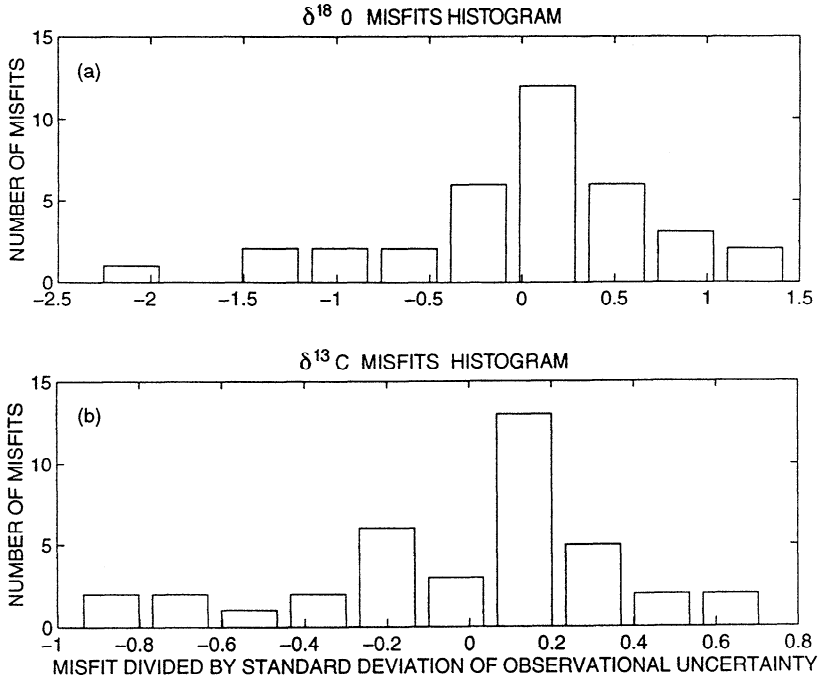

Figure 12. Histogram of the data misfits after minimization for $\delta^{18}O$ and $\delta^{13}C$, as in Figure 6, but for the LGM run 1.

as today. To explore alternative possibilities, we now ask whether a circulation can be found, differing significantly from the modern one while being consistent with the data. In particular, we test the hypothesis that the conventional scenario of a reduced flux of Lower NADW [*Boyle and Keigwin*, 1987; *Duplessy et al.*, 1988] is acceptable.

The prior estimate of the tracer field is given by the paleodata (as in paleocirculation estimate 1), and the prior circulation is the same as in the modern ocean in the interior, but the DWBC strength is reduced in the prior estimate by 50%. After minimization of the objective function (Figure 15), mass is again nearly perfectly conserved with normalized residuals smaller than 3×10^{-3} % everywhere (Figure 16a). Tracer residuals are all lower than 10% and of the order of a few tenths of a percent on average (Figures 16b, 16c, and 16d). Linear vorticity and thermal wind balances are well satisfied with residuals less than about 10% and of roughly 1% on average (Figures 16e and 16f). The characteristic times associated with the equation imbalances are very large (Table 1).

The posterior estimate of the tracer field is visually close to the data and to the field obtained with the full strength DWBC (compare Figure 17 with Figure 11 and see Figure 18). Here again, the tracer departures from the data are small and are deemed to be acceptable. The prior estimate of the circulation is only slightly modified by the inversion. The transports in the interior of the ocean are almost identical to their modern counterparts, and the transports in the DWBC remain 50% of the modern values in the deep levels of the model (compare Figure 19 with Figure 7). There is a southward flux of 8 ± 4 Sv between depths of 2 km and 5 km across 10°N (Figure 20), as distinct from the 14 ± 4 Sv of the scenario described in the previous section (Figure 14). The zonally integrated southward transport below 3 km depth across 50°N is 5 ± 3 Sv (Figure 20) instead of 9 ± 3 Sv in the previous scenario (Figure 14), and the flux of Lower NADW has been reduced by about 50% compared to the modern ocean solution.

At this stage, some simple conclusions can be drawn: the paleotracer data are incapable of distinguishing an LGM circulation like that of the modern ocean from one which conforms to the now-conventional scenario of a reduced flux of NADW. Although the problem is nonlinear, making generalizations difficult, it is characteristic of optimization problems which are nearly linear that if there is more than one solution, then there are typically an infinite number. About 10% of the eigenvalues of the Hessian matrix (matrix of the second partial derivatives) of the objective function almost vanish, which implies that the curvature of the objective function is very small in the direction of the associated eigenvectors [*Gill et al.*, 1981]. This small curvature means that the minimum of the objective function lies in flat valleys and that there probably are an infinity of points which minimize almost equally well the objective function. In other words, there are an infinity of ocean circulations that are equally consistent with the available paleotracers. Thus the general conclusion is that available passive, steady state tracer data provide only weak constraints on the LGM circulation.

In any model, however, which is anything less than global in scope, the question inevitably arises as to whether the regional results are not in some way inconsistent with data in the rest of the ocean. At the present time, any global model of the type we have been discussing would be so underconstrained by the LGM data base as to render it nearly useless.

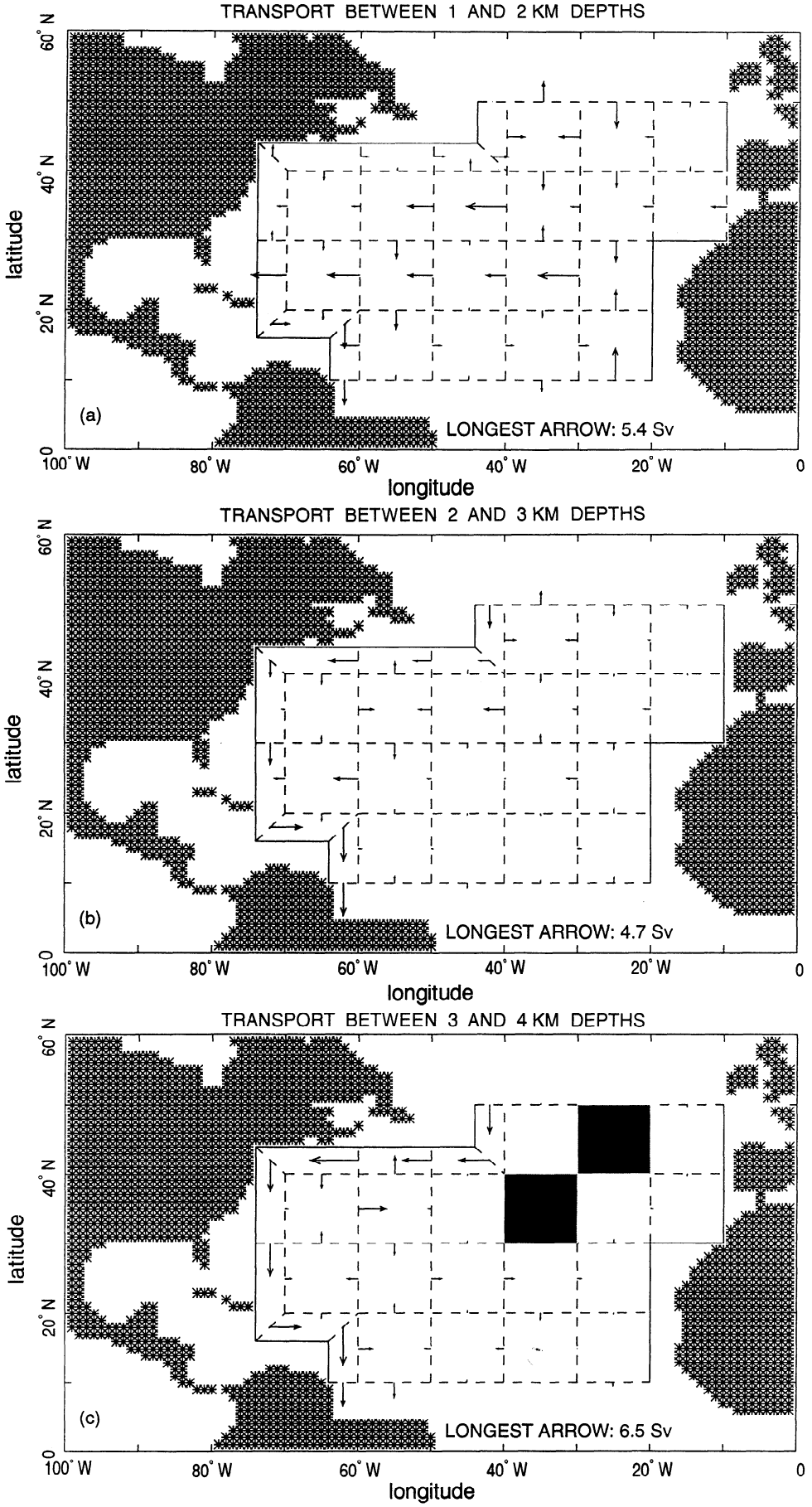

Figure 13. Horizontal transports (in Sverdrups) estimated by the model, as in Figure 7, but for the LGM run 1.

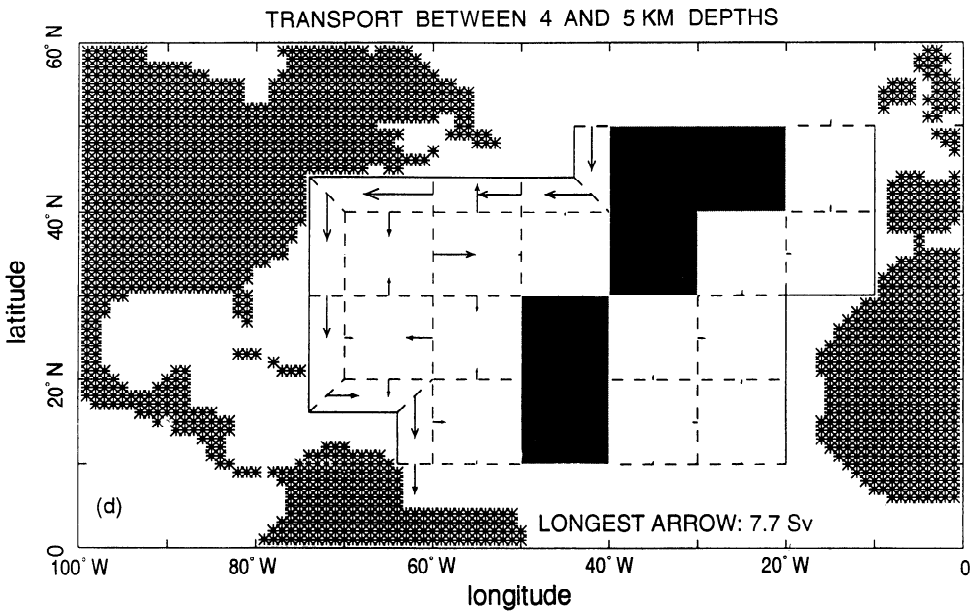

Figure 13. (continued)

There are, however, a few data in the South Atlantic, enough to suggest a brief attempt to test their consistency with the solutions we have obtained.

4. Consistency of the North Atlantic Model Estimates With the South Atlantic Data

It is not clear whether the low $\delta^{13}C$ values observed in the LGM Southern Ocean can be maintained at steady state in presence of a large input of high-$\delta^{13}C$ water from the North Atlantic. We thus now turn to examining whether the high NADW flux solution 1 is consistent with the LGM South Atlantic data, a calculation prototypical of that which may one day be possible for a global data set.

Because so few data exist for the South Atlantic, an elaborate representation is not justified, and a schematic five-box model is used to represent the deep circulation there (see Figure 21). As in the North Atlantic model, the South Atlantic basin is divided into four layers in the vertical. The upper waters are not explicitly modeled, but there are exchanges across the upper boundary of the model. The Atlantic sector of the

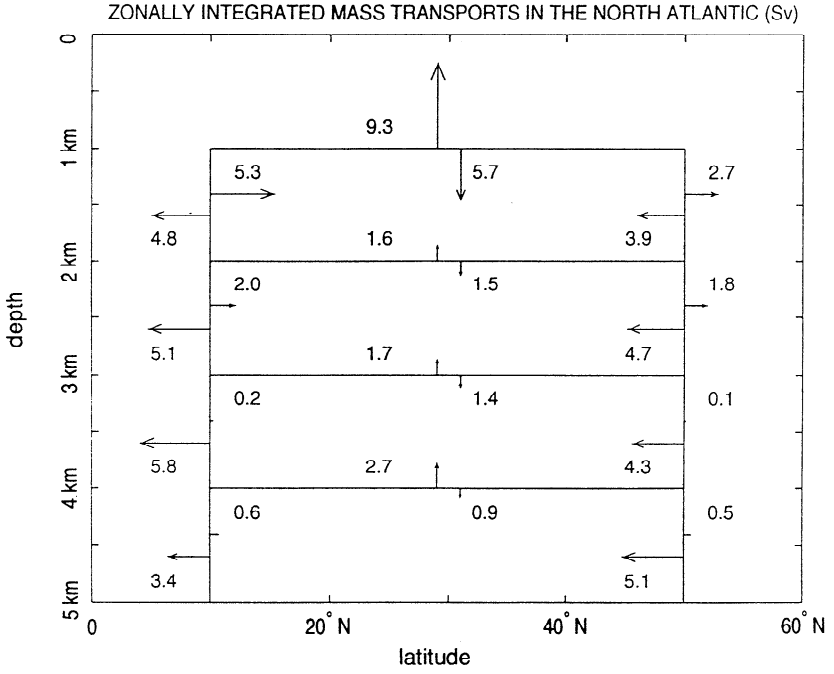

Figure 14. Zonally integrated mass transports in the North Atlantic (in Sverdrups), as in Figure 8, but for the LGM run 1.

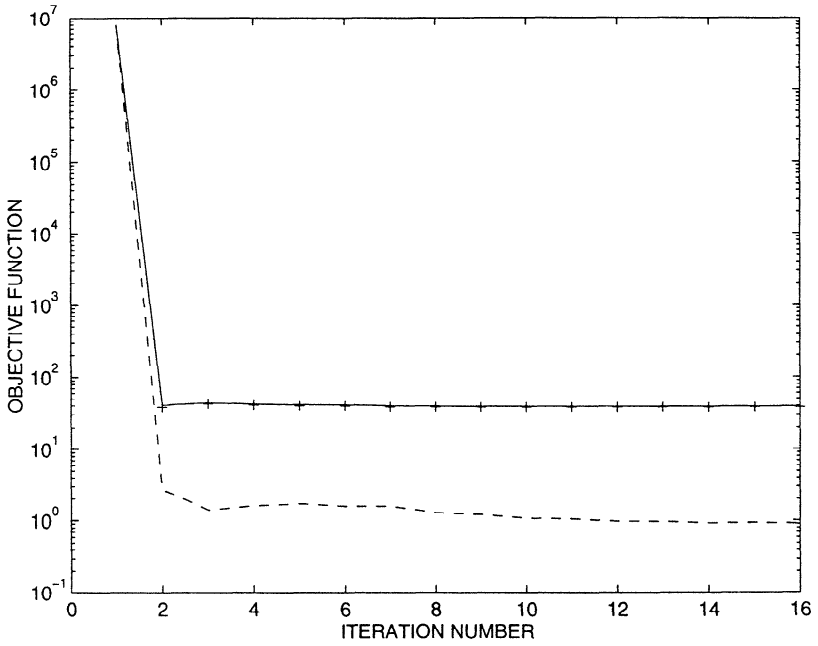

Figure 15. Objective function versus the number of iterations, as in Figure 9, but for the LGM run 2 (flux of Lower NADW reduced to half its modern value).

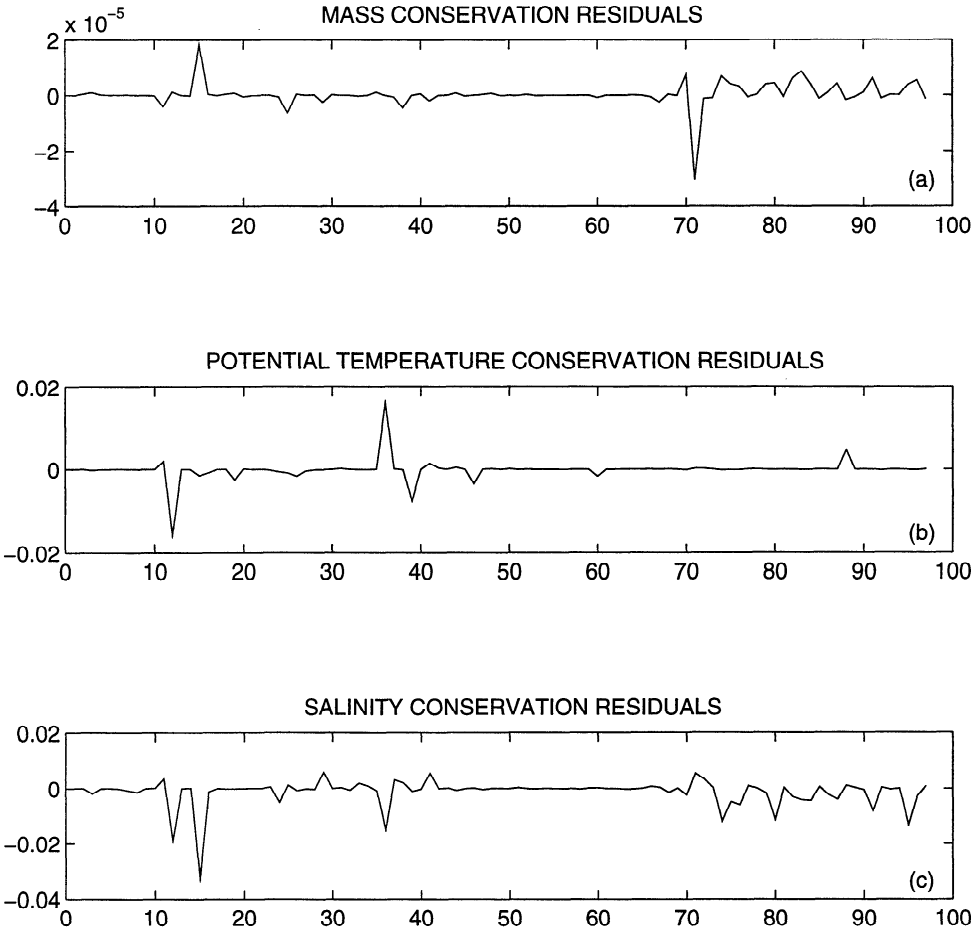

Figure 16. Residuals after minimization, as in Figure 4, but for the LGM run 2.

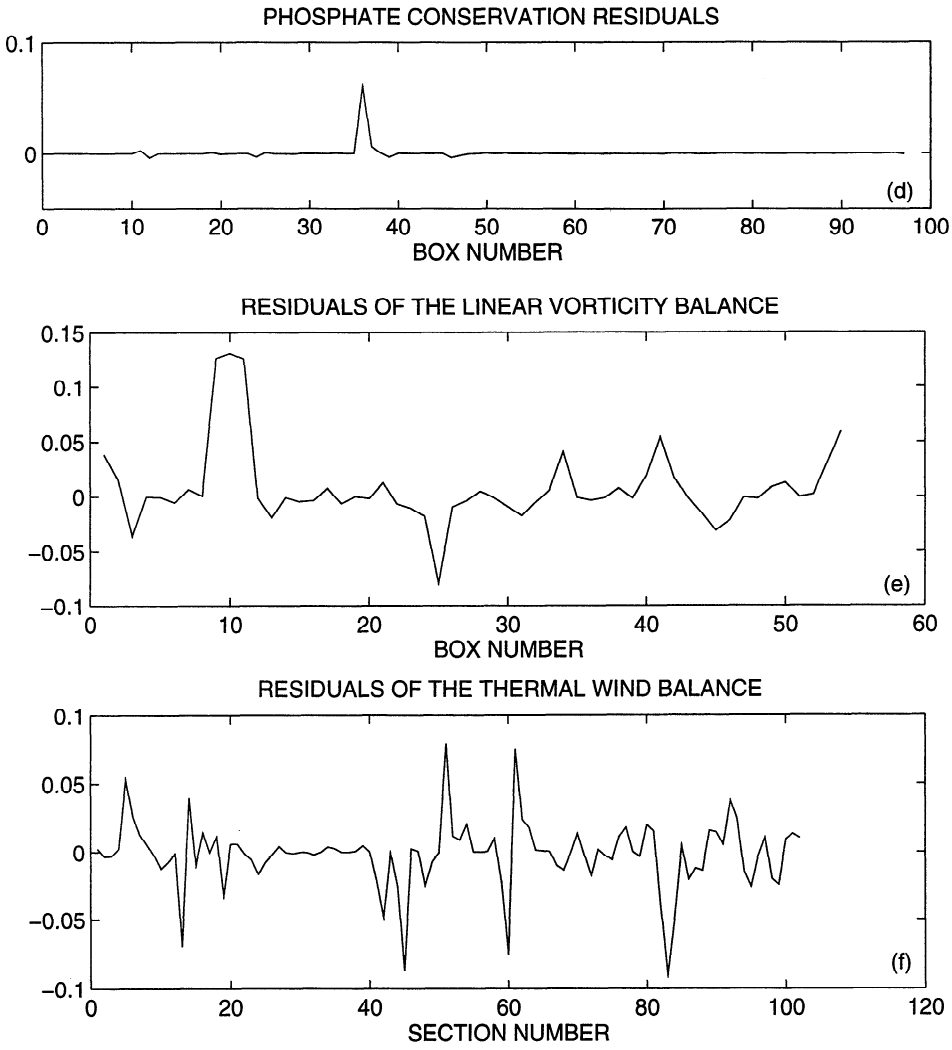

Figure 16. (continued)

Circumpolar Current below 1 km depth is represented by a single box. Some water enters this box through the Drake Passage, and some leaves it around the Cape of Good Hope. The tracer characteristics of upper waters and Drake Passage water, as well as the fluxes leaving and entering the model domain, are treated as unknown variables and estimated as part of the solution. However, the fluxes of mass and tracers exchanged with the North Atlantic come from the North Atlantic model output and are fixed parameters, the goal being to check their consistency with the South Atlantic data.

Only mass, ^{13}C, and potential temperature (computed from $\delta^{18}O$ data) conservation are imposed. The effects of biology are neglected. Were they to be taken into account, more degrees of freedom would be introduced into the model, making it easier to combine the fluxes computed from the North Atlantic model with the South Atlantic data. Because of the model crudity, no dynamics are included; the model is purely kinematic.

The model appears mathematically as 15 equations (10 being nonlinear) in 36 unknowns (tracer concentrations and mass transports). Because the problem is so small, it was solved using the constrained optimization technique known as "minimax" [*Gill et al.*, 1981]. This method minimizes the maximum equation imbalance, rather than a sum-of-squares objective function. The method is convenient because it tends to minimize all the equation imbalances to the same level so the constraints are equally well satisfied in every box, avoiding the potential problem of having large imbalances concentrated in a few boxes. Formally, the optimization problem is

$$\begin{aligned} \min J = \min (\max | f_i(x_1, \ldots, x_{36}) |) \\ 1 \le i \le 15 \\ l_1 \le x_1 \le u_1 \\ \vdots \\ l_{36} \le x_{36} \le u_{36} \end{aligned} \qquad (10)$$

where J is the objective function, f_i represents the equation imbalances, x_i represents the elements of the state vector, and l_i and u_i are the lower and upper bounds of x_i. The bounds imposed on the state vector represent the observational uncertainties. More details are given by *LeGrand* [1994].

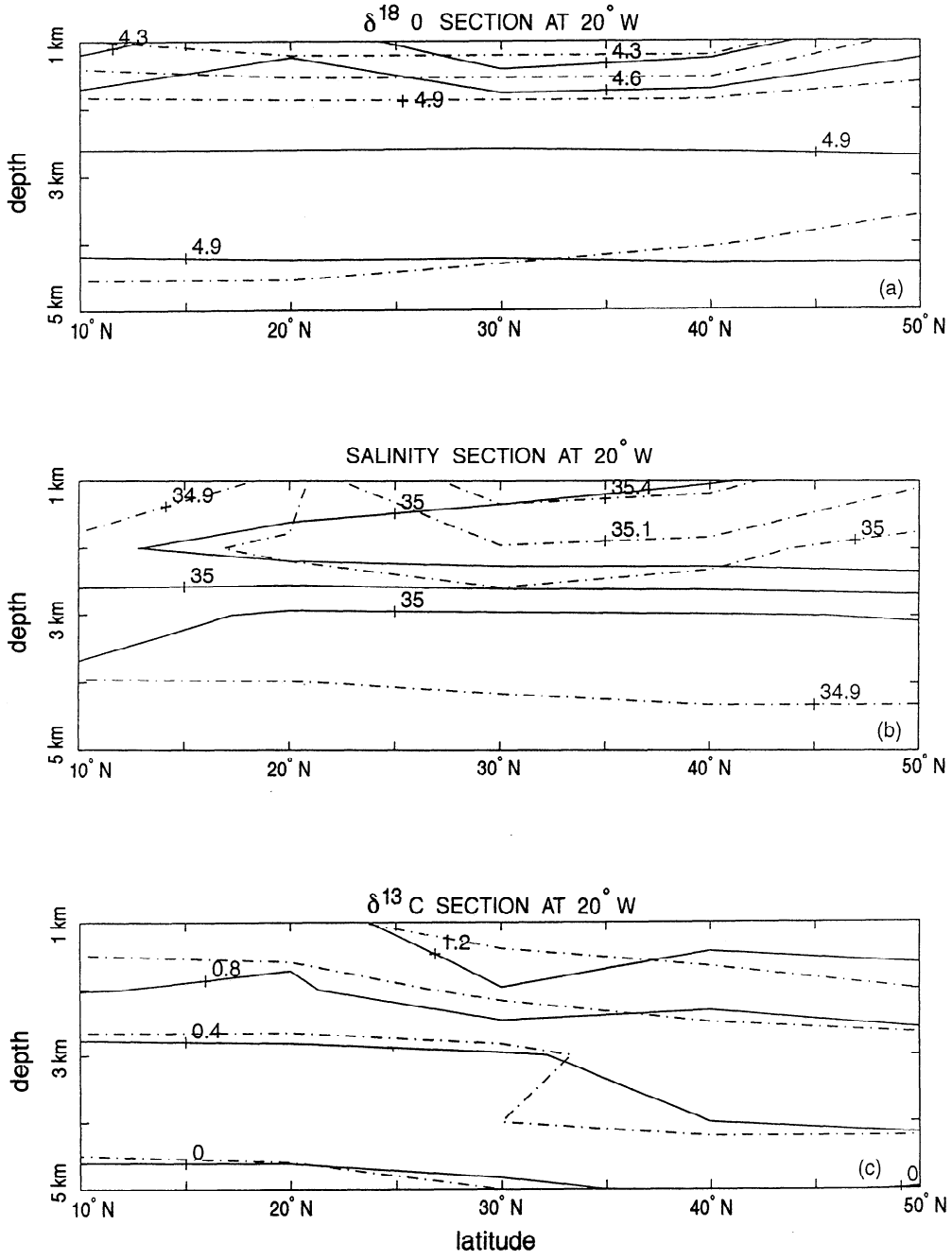

Figure 17. Meridional sections of $\delta^{18}O$ (per mil), salinity (Practical Salinity Scale), and $\delta^{13}C$ (per mil), as in Figure 11, but for the LGM run 2.

The fluxes across the northern boundary of the model are computed from the output of paleoestimate 1. Because the South Atlantic tracer distribution is poorly constrained, tracer concentrations are relatively free to vary so that after optimization, conservation equations are almost perfectly satisfied (residuals almost zero). The transports indicated (Figure 22) seem reasonable. About 50 Sv enter the Atlantic sector of the Circumpolar Current through the Drake Passage and leave it south of the Cape of Good Hope.

Mackensen et al. [1993] suggested that the LGM $\delta^{13}C$ data in the deep Circumpolar Current should be about 0.6 ‰ lower than modern values, which give a LGM $\delta^{13}C$ value of about -0.3 ‰. We took the *Lohmann and Lohmann* [1994] $\delta^{13}C$ profile as a typical profile for the South Atlantic data. This profile indicates a $\delta^{13}C$ value of about 1.4 ‰ at 800 m depth. However, most other data sets [e.g., *Sarnthein et al*, 1994] suggest smaller values in the LGM upper ocean. We thus imposed an upper bound of 1 ‰ on this value.

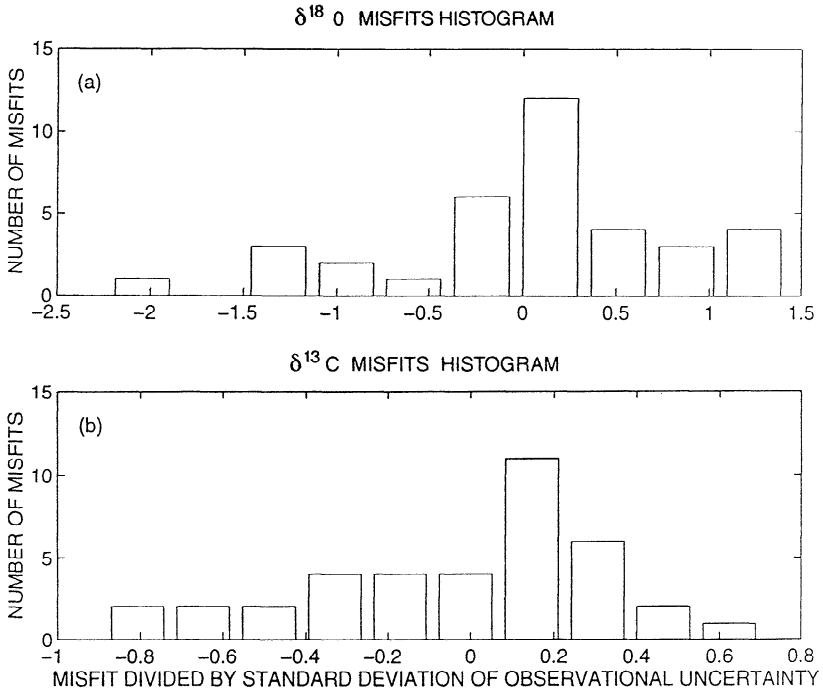

Figure 18. Histogram of the data misfits after minimization for $\delta^{18}O$ and $\delta^{13}C$, as in Figure 12, but for the LGM run 2.

The $\delta^{13}C$ distribution estimated by the model (Figure 22) is consistent with the prior estimate of the vertical profile of $\delta^{13}C$, and we conclude that the South Atlantic LGM paleodata do not conflict with the high NADW flux solution 1. Because the data density in the Indian, Pacific, and Southern Oceans is even lower than in the South Atlantic, we do not expect data from these areas to be any more incompatible with the modern flux of NADW than the South Atlantic data.

5. Summary and Discussion

5.1. Summary

The circulations discussed here differ from previous attempts to make inferences from paleodata in a number of ways. They are consistent not only with the paleodata but also with realistic physics, in the guise of the thermal wind

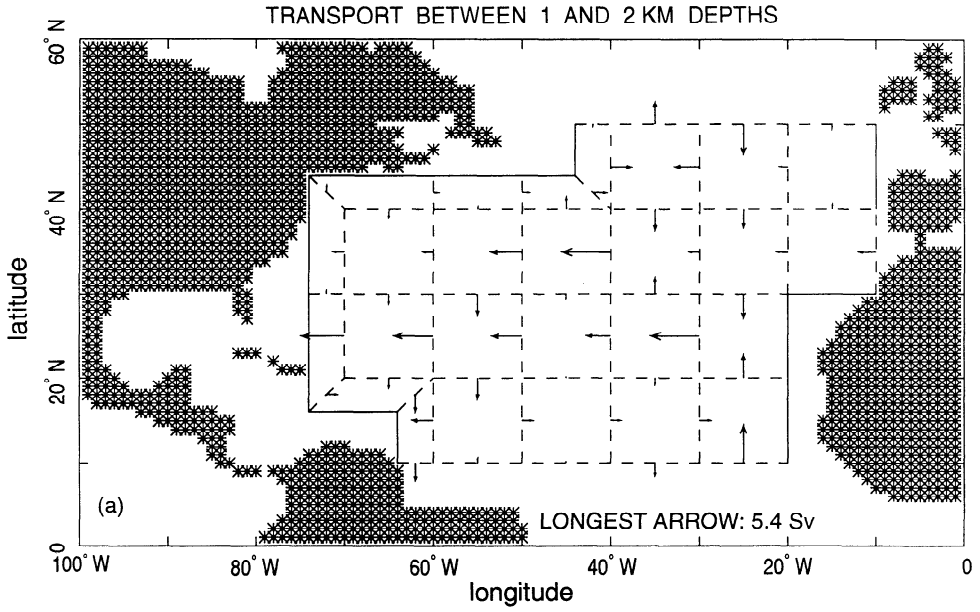

Figure 19. Horizontal transports (in Sverdrups) estimated by the model, as in Figure 7, but for the LGM run 2.

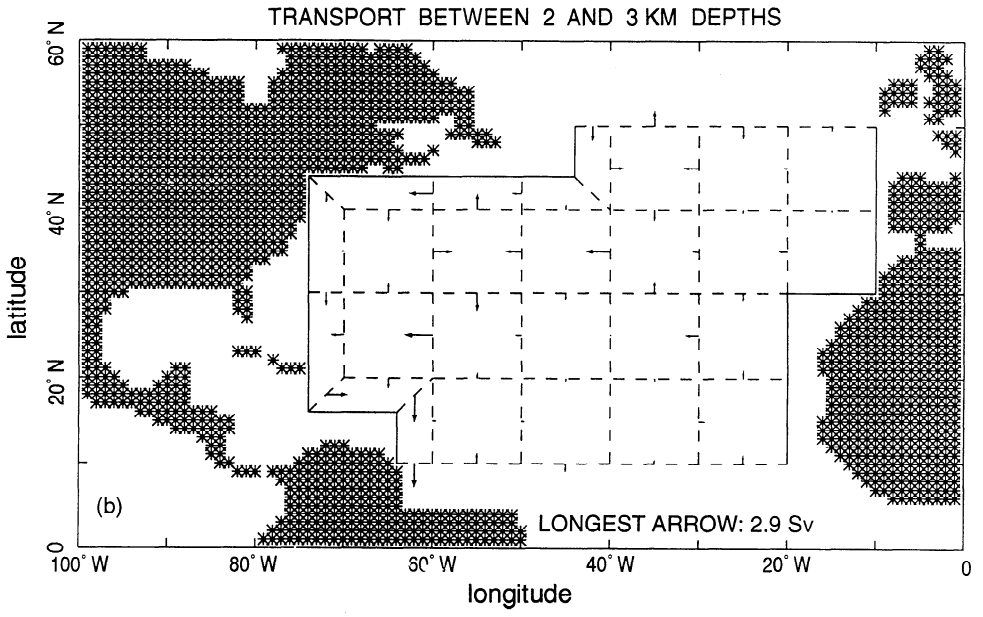

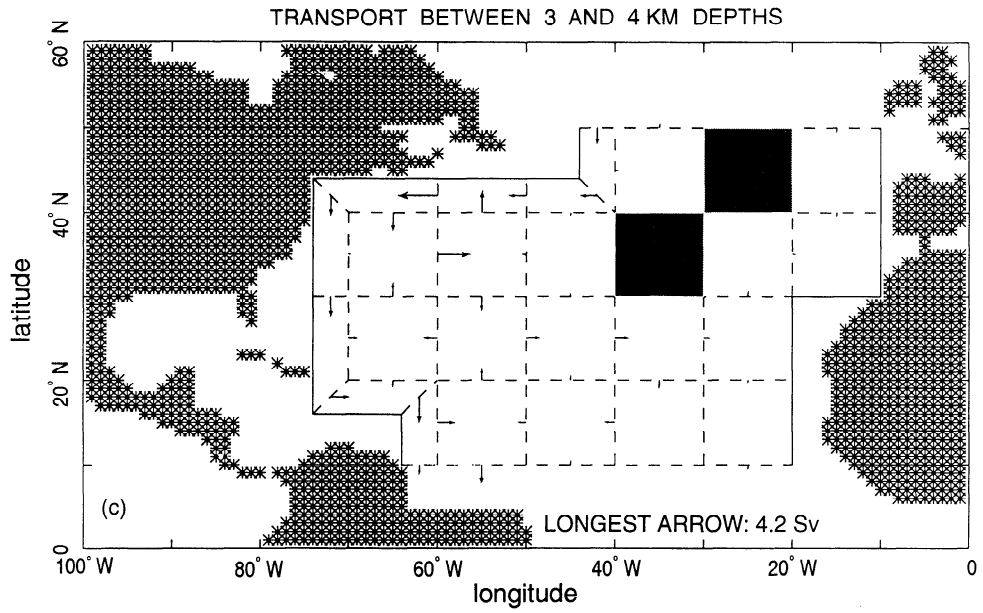

Figure 19. (continued)

(geostrophy) and potential vorticity conservation. Previous box model computations [*Keir*, 1988; *Broecker et al.*, 1990; *Michel*, 1991] did not include these constraints. The present results also differ from the previous ones in retaining a full three-dimensional representation of the ocean circulation, rather than collapsing the data into a two-dimensional model with a very small number of degrees of freedom.

The distinction has been made throughout this work between the depiction of the water mass distribution and the estimation of the oceanic circulation. The water mass distribution inferred from $\delta^{13}C$ data can be interpreted to show that the volume of AABW extended farther north and that the volume of Lower NADW was reduced during the LGM, compared to the modern ocean. However, the location of the water-mass boundary depends on knowledge of end-member values which are poorly known, and the differences between the glacial and the modern water mass distributions cannot be quantified. More $\delta^{13}C$ data are needed close to the regions of formation of deep water in order to constrain the end-members.

Two different oceanic circulations were found to be consistent with the observed distribution of $\delta^{13}C$ and $\delta^{18}O$ in the LGM Atlantic. The first one is indistinguishable from the

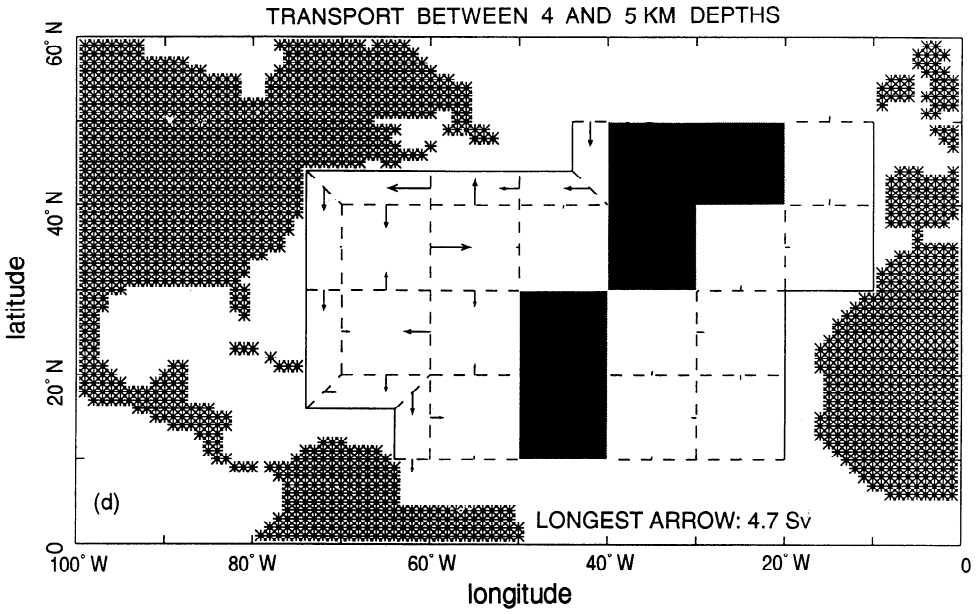

Figure 19. (continued)

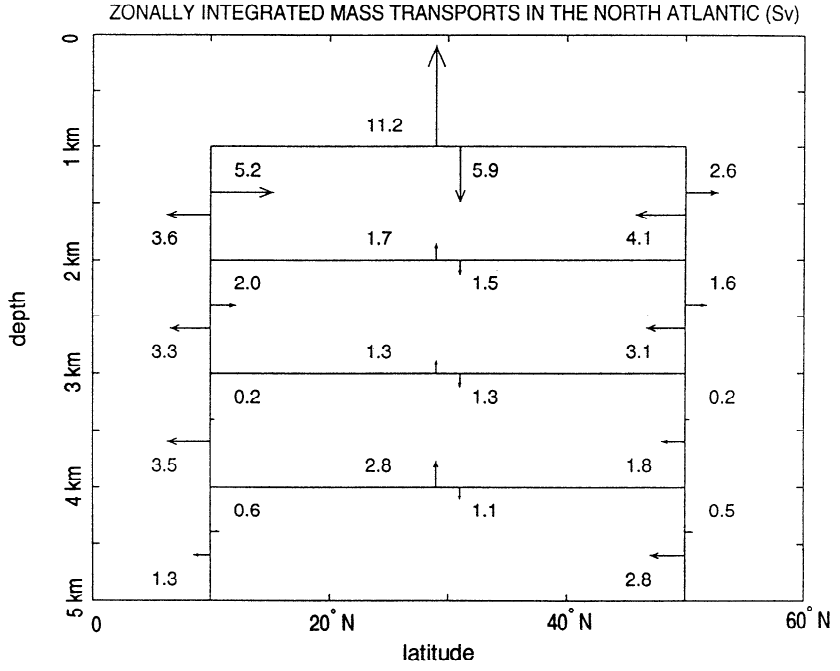

Figure 20. Zonally integrated mass transports in the North Atlantic (in Sverdrups), as in Figure 8, but for the LGM run 2.

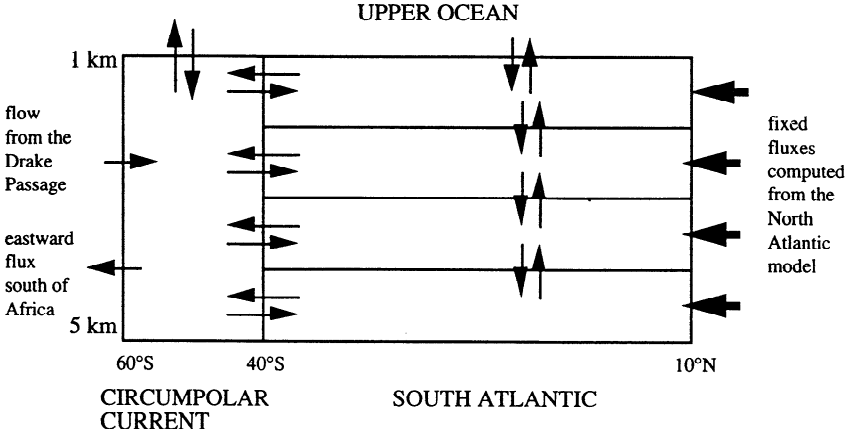

Figure 21. Kinematic five-box model of the deep South Atlantic.

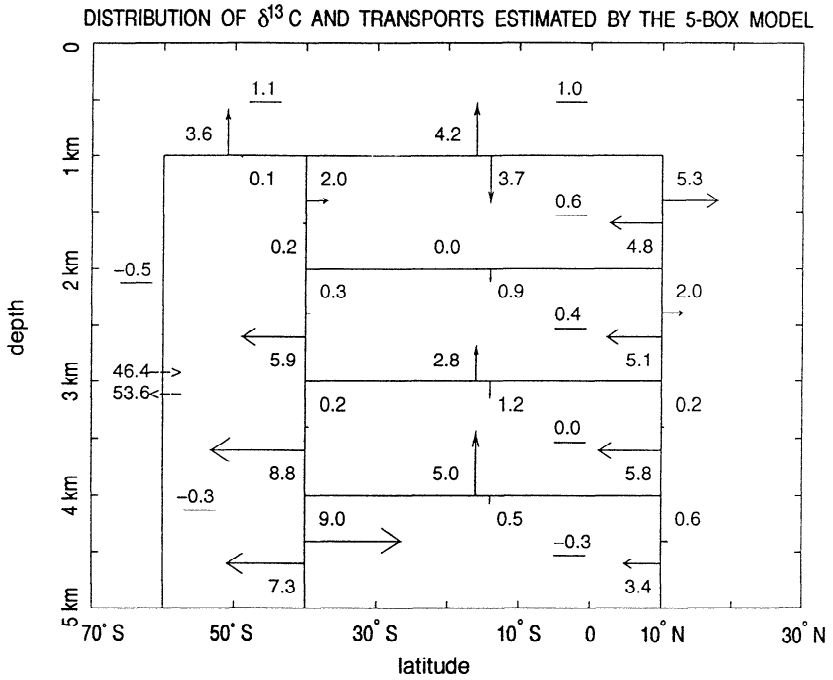

Figure 22. Northward and southward zonally integrated transports (in Sverdrups) in the South Atlantic for the LGM run 1 estimated by the kinematic five-box model (forced with fluxes across 10°N computed by the inverse model of the North Atlantic). Volume fluxes into and out of Atlantic sector of Circumpolar Current are in reality perpendicular to the meridional plan. Arrows corresponding to these fluxes are not scaled. Underlined numbers represent the $\delta^{13}C$ values obtained by the box model in each box and at the boundaries of the model domain.

modern circulation, which suggests that significant circulation changes are not required by the paleodata. The second one reproduces the now-conventional scenario of a reduced flux of Lower NADW. The two circulation schemes are equally acceptable, and it is not possible to draw conclusions from the available data base concerning the rate of ventilation of the deep ocean during the LGM.

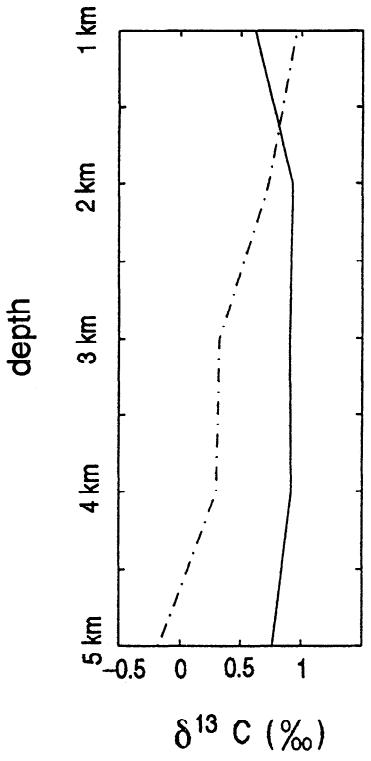

5.2. What Sets the Tracer Concentrations?

The lower $\delta^{13}C$ values in the deep Atlantic during the LGM (Figure 23) arise from different mechanisms in scenarios 1 and 2. In scenario 1, with the flux of NADW close to its modern value, the lowered concentrations arise from the lowered preformed $\delta^{13}C$. In scenario 2, they arise from the reduced flux of relatively enriched $\delta^{13}C$ across 50°N.

The mechanism involved in paleoscenario 1 can be identified in the kinematic box model of the South Atlantic. According to the box model, low $\delta^{13}C$ values (-0.3 ‰) are advected from the Southern Ocean into the bottom layer of the South Atlantic (Figure 22) and then into the deep layers of the North Atlantic. Despite some dilution, the water entering the North Atlantic is sufficiently depleted in $\delta^{13}C$ so that it is not necessary to reduce the flux of NADW across 50°N to obtain low $\delta^{13}C$ values in this basin (note that a $\delta^{13}C$ value of -0.3 ‰ in

Figure 23. Vertical profiles of $\delta^{13}C$ at 20°W, 20°N estimated by the inverse model of the North Atlantic. Solid line represents the modern ocean profile (calculated from phosphate values). Dotted-dashed line represents the profile calculated in the LGM run 1 (modern circulation as prior value). The observation that intermediate waters are enriched in $\delta^{13}C$ and deep waters are depleted in $\delta^{13}C$ in the North Atlantic during glacial times, compared to modern times, is reproduced in the model estimates.

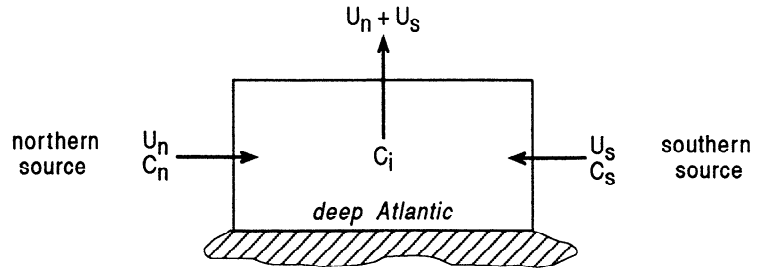

Figure 24. One-box model of the deep Atlantic with two sources of tracer.

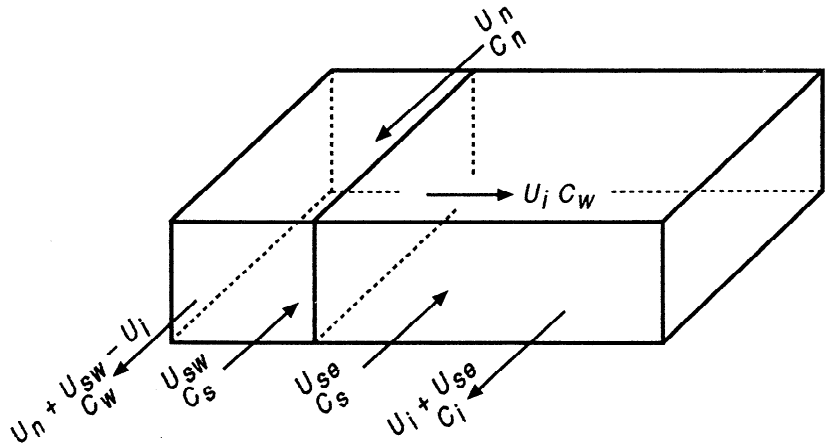

Figure 25. Two-box model of the Atlantic. Interior of the Atlantic is fed from a southern source and a recirculation from the western boundary, and there is no interior flow through the northern boundary. U_{sw} and $U_n+U_{sw}-U_i$ represent the northward flow of AABW (west of the Mid-Atlantic Ridge) and the southward flow of NADW across the southern boundary of the Atlantic. U_{se} represents the northward flow of AABW east of the Mid-Atlantic Ridge. It is assumed that U_{sw} and U_{se} advect water masses with the same tracer composition.

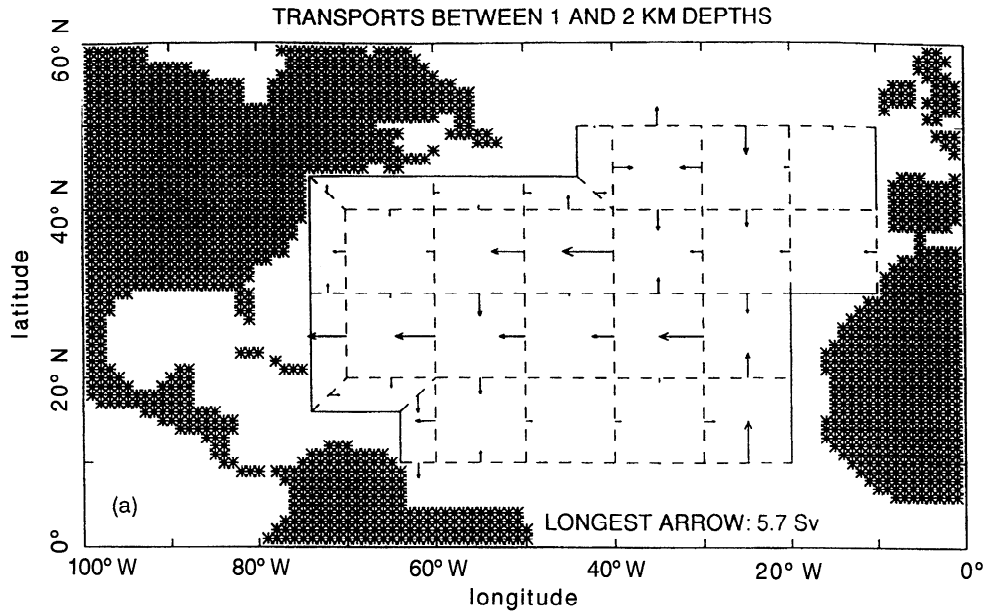

Figure 26. Horizontal transports (in Sverdrups), as in Figure 7, but for the "phosphate-only" modern ocean run.

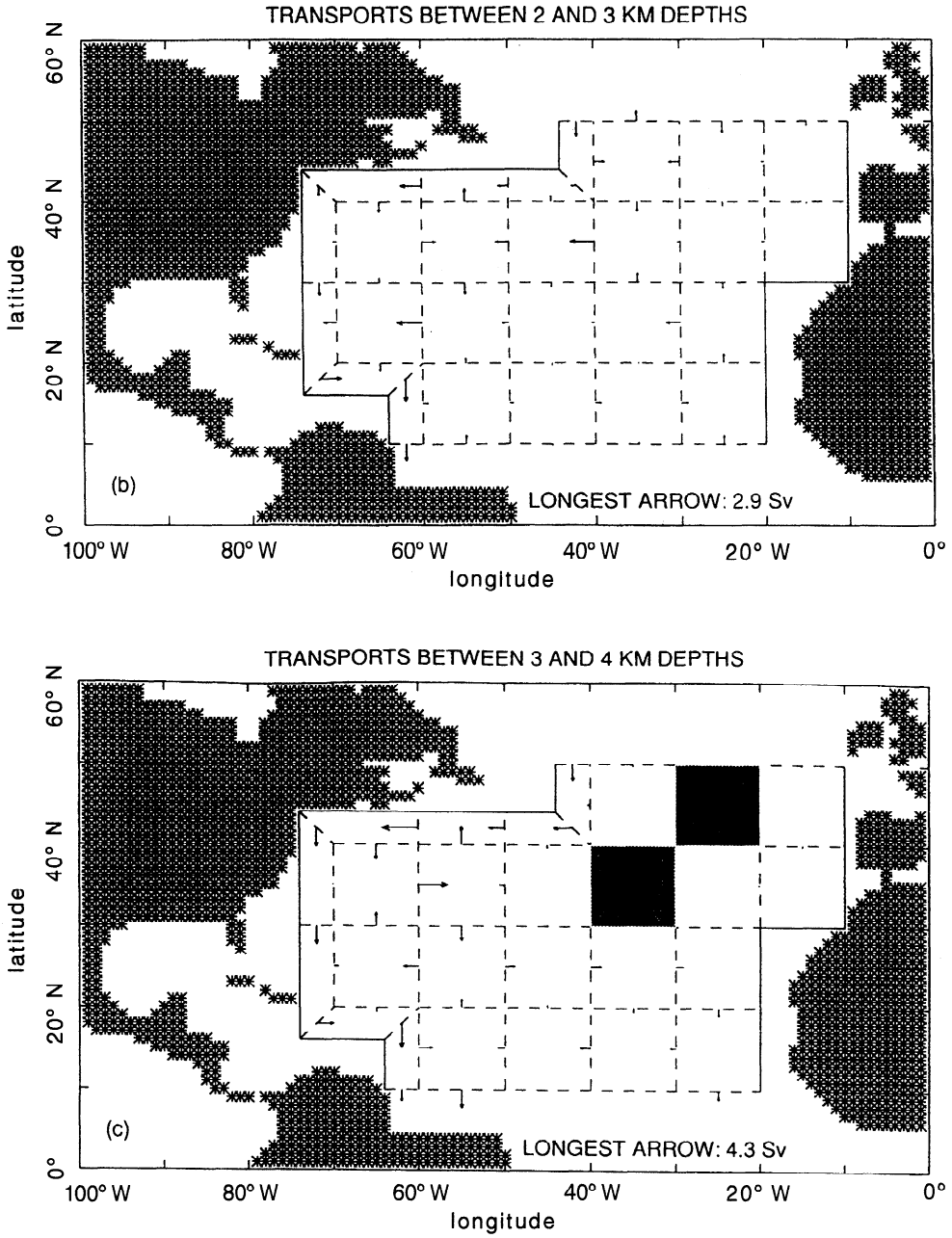

Figure 26. (continued)

the glacial Southern Ocean is not an extreme estimate and that even more negative values are plausible).

A reduced flux of NADW during glacial time, hence a weaker input of high $\delta^{13}C$ water, is often used as an explanation of the lower Southern Ocean $\delta^{13}C$ levels during the LGM. There is confusion in this explanation between the inventory of the water masses and their rates of input. The results of the inverse model calculations show that water mass inventory and water mass flux are two separate issues. Thus the lower $\delta^{13}C$ levels in the glacial Southern Ocean indicate a smaller amount of NADW-type water present in this basin, not a reduced flux of NADW, and they do not require a LGM circulation different from the present one.

5.3. Passive Tracers Only Weakly Constrain the Ocean Circulation

A "standing crop" of a passive, stable tracer distribution is by itself incapable of producing values for the rate at which the tracer is carried through the volume; there must be some externally prescribed rate-setting mechanism, i.e., a "clock", such as provided by the geostrophic constraints. This idea can

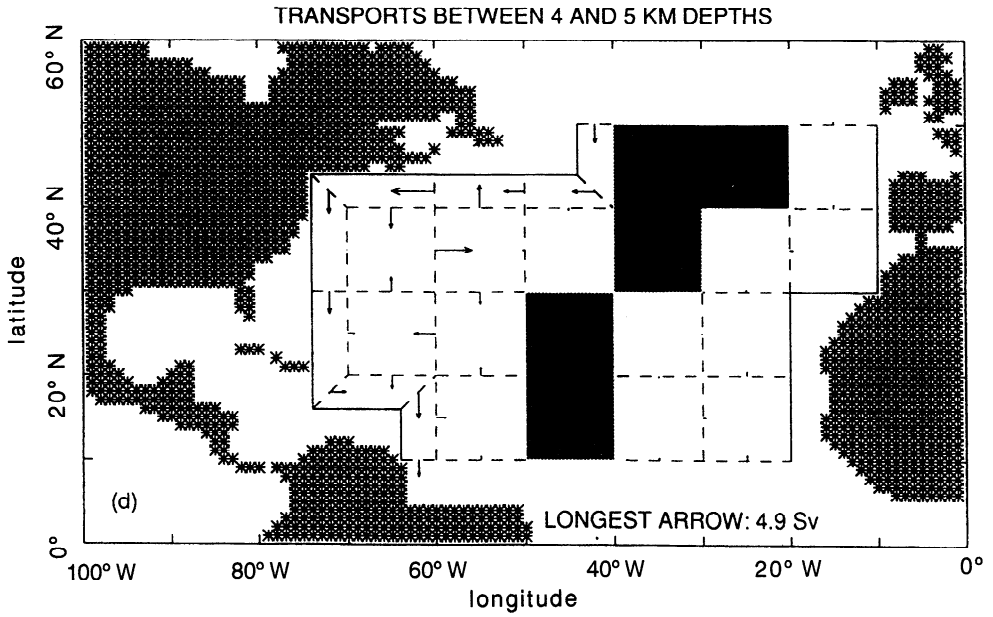

Figure 26. (continued)

be illustrated by a simple one-box model of the deep Atlantic (Figure 24). Tracer conservation in the interior of the box can be written in terms of contributions of Northern (U_n) and Southern (U_s) sources

$$\frac{U_s}{U_n} = \frac{C_n - C_i}{C_i - C_s} \tag{11}$$

C_n and C_s represent the northern and southern end-members and C_i a typical concentration in the middle of the basin. Relation (11) shows that in the box model, U_n and U_s can be multiplied by any arbitrary constant without affecting the tracer distribution, and therefore the absolute rates of circulation cannot be determined from tracer data only. In the modern ocean, this difficulty is overcome thanks to the thermal wind relations, which set the overall circulation rate once mass conservation is prescribed. In the LGM ocean, density gradients cannot be estimated because salinity gradients are unknown and temperature gradients are poorly determined. Even if drastic assumptions are made about the salinity and the $\delta^{18}O$

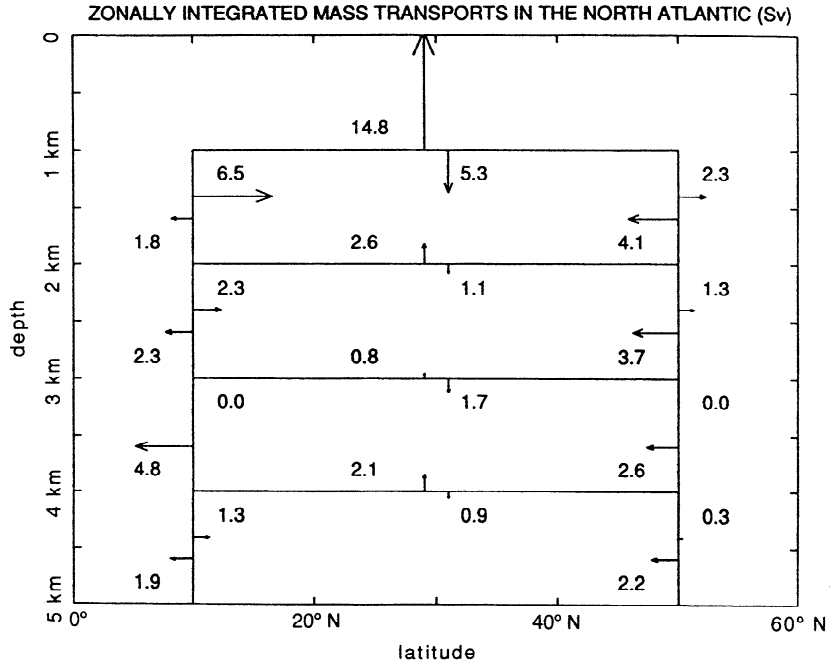

Figure 27. Zonally integrated mass transports in the North Atlantic (in Sverdrups), as in Figure 8, but for the "phosphate-only" modern ocean run.

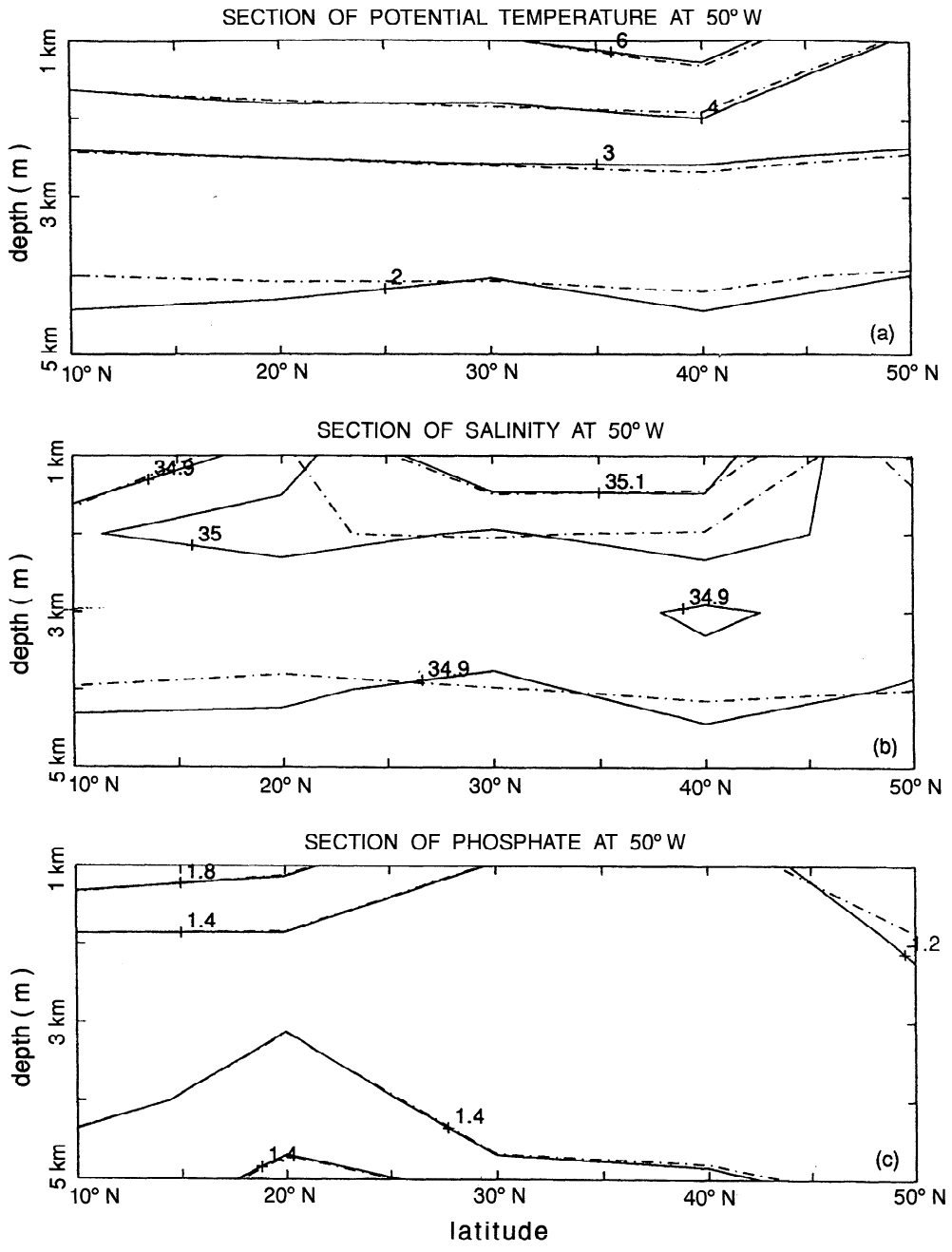

Figure 28. Meridional sections of potential temperature (in degrees Celsius), salinity (Practical Salinity Scale), and phosphate (in micromoles per liter), as in Figure 5, but for the "phosphate-only" modern ocean run.

of sea water, as in paleocirculation estimates 1 and 2, the uncertainty of the temperature field, about 1°C, is too large to allow the determination of density gradients in the deep ocean. In such a situation, the thermal wind cannot be used to set the circulation rate.

It has been suggested [*Boyle and Keigwin*, 1982] that one could at least estimate the rate of production of NADW relative to AABW from steady tracers, as in relation (11). Such calculations, however, succeed only if the ocean is represented by a single box. To illustrate the point, consider a two-box model, which can be thought of as a representation of the Atlantic treating the DWBC and the interior of the ocean separately (Figure 25). Let C_s and C_n be the southern and northern end-members of C, let C_w and C_i be the tracer concentrations in the DWBC and in the interior of the Atlantic, let U_{sw}, U_{se}, and U_n be the volume transports across the southwestern, southeastern, and northern boundaries of the model, and let U_i be the volume transport from the DWBC into the interior of

the basin. The tracer budgets for the two boxes can be written as

$$\frac{U_{sw}}{U_n} = \frac{C_n - C_w}{C_w - C_s} \tag{12}$$

and

$$\frac{U_{se}}{U_i} = \frac{C_w - C_i}{C_i - C_s} \tag{13}$$

Combining the two expressions, we obtain

$$\frac{U_s}{U_n} = \frac{U_{sw} + U_{se}}{U_n} = \frac{C_n - C_w}{C_w - C_s} + \frac{U_t}{U_n} \times \frac{C_w - C_t}{C_i - C_s} \tag{14}$$

Relation (14) shows that one can no longer determine even the ratios of the volume fluxes because U_t/U_n is unknown.

Another weakness of steady passive tracers is that they provide only local constraints on the ocean circulation. According to relation (12), the tracer concentration in the eastern basin of the Atlantic, C_i, does not directly constrain the ventilation of the western basin. Direct information about the tracer distribution in the western Atlantic is required for that purpose. The local character of tracer constraints partly explains why paleocirculations 1 and 2 are two equally acceptable solutions. These circulations and the corresponding tracer distributions are almost identical in the eastern Atlantic and thus are equally consistent with the bulk of the data base. The only differences are in the DWBC where the data are too scarce to distinguish between the two solutions.

5.4. Modern Ocean Circulation Estimate With Passive Tracer Data Only

The inadequate sampling of the paleotracer distribution does not suffice to explain the ambiguity of the determination of the glacial circulation. The same ambiguity occurs with well-sampled modern tracer data when the geostrophic constraints are not available. To illustrate this point, the inverse model of the North Atlantic was run using modern phosphate data as the only observational constraints. As mentioned above, in the absence of observational constraints on temperature and salinity, the geostrophic equations cannot be used to set the circulation rate. In the "phosphate-only" run, the temperature, salinity, and phosphate distributions were initialized by the modern-reference property distributions. Temperature and salinity were free to vary so they did not constrain the solution. The phosphate distribution was required to remain as close as possible to the initial estimate.

To verify that a reduced flux of NADW is consistent with the modern-reference phosphate distribution, the circulation was initialized by the modern-reference circulation in the interior of the basin and by the modern-reference transports divided by 2 in the DWBC. The inversion did not much modify this initial circulation, and the final circulation corresponds to a flux of NADW significantly smaller than in the modern-reference circulation (compare Figures 26 and 27 with Figures 7 and 8). The phosphate distribution after inversion, however, is almost identical to that estimated in the modern-reference solution (Figure 28). Thus, in the absence of other constraints, both the modern-reference circulation and a reduced flux of NADW are consistent with the modern phosphate distribution. Other data are needed to distinguish between the two rates of circulation. This result cannot be directly extrapolated to the problem of estimating the paleocirculation because no temperature constraints were used in the "phosphate-only" run, but it clearly indicates that circulation rates cannot be estimated from passive tracer data alone.

5.5. Perspectives

To proceed from the present state of uncertain knowledge to a more definitive picture of the LGM circulation requires a number of improvements in the data base. Most important is the provision of a "clock", provided in the modern ocean primarily by the geostrophic relationship. Inference of the LGM density field with accuracy and spatial sampling adequate to deduce the density shear or well-distributed measurements of a radioactive tracer such as ^{14}C would permit deduction of overall rates of water and property fluxes. One requires sampling of all of the data types adequate to distinguish at least the eastern, western, and western boundary current regions of the North Atlantic. Whether such new data are physically possible, given the realities of core sampling, is not clear. To go beyond the study of an LGM steady state and a modern steady state to a study of the transition between them, with time variations in the flow, will be even more demanding of the database.

Acknowledgments. This work was supported in part by the U.S. National Science Foundation under grant OCE-9205942. Jochem Marotzke gave helpful advice on the model numerics, and discussions with John Marshall, Eric Sundquist, and Bruce Warren were very useful. We thank Pat Lohmann, Bill Curry, and Lloyd Keigwin for making unpublished data available to us. We are grateful to Edward Boyle, who although he does not entirely agree with the conclusions drawn here, was invaluable in his guidance through the paleoceanographic data sets.

References

Boyle, E.A, Cadmium and $\delta^{13}C$ paleochemical ocean distributions during the stage 2 glacial maximum, *Annu. Rev. Earth Planet. Sci., 20*, 245-287, 1992.

Boyle, E.A., and L.D. Keigwin, Deep circulation of the North Atlantic over the last 200,000 years: Geochemical evidence, *Science, 218*, 784-787, 1982.

Boyle, E.A., and L.D. Keigwin, North Atlantic thermohaline circulation during the past 20,000 years linked to high latitude surface temperature, *Nature, 330*, 35-40, 1987.

Broecker, W.S., and T.-H. Peng, *Tracers in the Sea*, 690 pp., Eldigio, Palisades, N.Y., 1982.

Broecker, W.S., T.-H. Peng, S. Trumbore, G. Bonani, and W. Wolfli, The distribution of radiocarbon in the glacial ocean, *Global Biogeochem. Cycles, 4*, 103-117, 1990.

Charles, C.D., and R.G. Fairbanks, Evidence from Southern Ocean sediments for the effect of North Atlantic deep-water flux on climate, *Nature, 355*, 416-419, 1992.

Curry, W.B., J.-C. Duplessy, L.D. Labeyrie, and N.J. Shackleton, Changes in the distribution of $\delta^{13}C$ of deep water ΣCO_2 between the last glaciation and the Holocene, *Paleoceanography, 3*, 317-341, 1988.

Duplessy, J.C., N.J. Shackleton, R.G. Fairbanks, L.D. Labeyrie, D. Oppo, and N. Kallel, Deepwater source variations during the last climatic cycle and their impact on the global deepwater circulation, *Paleoceanography, 3*, 343-360, 1988.

Fukumori, I., F. Martel, and C. Wunsch, The hydrography of the North Atlantic in the early 1980's. An atlas, *Prog. Oceanogr., 27*, 1-100, 1991.

Gill, P.E., M.H. Murray, and M.H. Wright, *Practical Optimization*, 401 pp., Acad. P., San Diego, Calif., 1981.

Keigwin, L.D., and E.A. Boyle, Late Quaternary paleochemistry of high-latitude surface waters, *Palaeogeogr. Palaeoclimatol. Palaeoecol., 73*, 85-106, 1989.

Keir, R.S., On the late Pleistocene ocean geochemistry and circulation, *Paleoceanography, 3*, 413-446, 1988.

Kroopnick, P.M., The distribution of ^{13}C of ΣCO_2 in the world oceans, *Deep Sea Res., 32*, 57-84, 1985.

Labeyrie, L.D., J.-C. Duplessy, J. Duprat, A. Juillet-Leclerc, J. Moyes, E. Michel, N. Kallel, and N.J. Shackleton, Changes in the vertical structure of the North Atlantic Ocean between glacial and modern times, *Quat. Sci. Rev., 11*, 401-413, 1992.

LeGrand, P., What do paleo-geochemical tracers tell us about the deep ocean circulation during the Last Ice Age?, Ph.D. thesis, p. 194, Massachusetts Inst. of Technol.-Woods Hole Oceanogr. Inst., Joint Program in Oceanography, Cambridge, June 1994.

Lohmann, G.P., and K.C. Lohmann, Vertical $\delta^{13}C$ gradient in the South Atlantic during the last glacial maximum recorded in benthic and planktonic foraminifera, paper presented at the symposium "The South Atlantic: Present and past circulation", Oceanogr. Soc., Bremen, Germany, 1994.

Mackensen, A., H.-W. Hubberten, T. Bickert, G. Fisher, and D.K. Futterer, The $\delta^{13}C$ in benthic foraminiferal tests of *Fontbiota Wuellerstorfi* (Schwager) relative to the $\delta^{13}C$ of dissolved inorganic carbon in Southern Ocean deep water: Implications for glacial ocean circulation models, *Paleoceanography, 6*, 587-610, 1993.

Martel, F., and C. Wunsch, The North Atlantic circulation in the early 1980s - An estimate from inversion of a finite-difference model, *J. Phys. Oceanogr., 23*, 898-924, 1993.

Mathworks, Inc., *MATLAB, 4.0, Reference Guide*, Natick, Mass., 1992.

McCartney, M.S., S.L. Bennett, and M.E. Woodgate-Jones, Eastward flow through the Mid-Atlantic Ridge at 11°N and its influence on the abyss of the eastern basin, *J. Phys. Oceanogr., 21*, 1089-1121, 1991.

Mercier, H., Determining the general circulation of the ocean: A nonlinear inverse problem, *J. Geophys. Res., 94*, 5103-5109, 1986.

Mercier, H., A study of the time-averaged circulation of the ocean in the western North-Atlantic by simultaneous inversion of hydrographic and current meter data, *Deep Sea Res., Part A, 36*, 297-313, 1989.

Michel, E., L'ocean au dernier maximum glaciaire: Le cycle du carbone et la circulation. Contraintes isotopiques et modelisation, Ph.D. thesis, p. 191, Univ. de Paris-Sud, Centre d'Orsay, Orsay, 1991.

Mix, A.C., The oxygen-isotope record of glaciation, in *The Geology of North America*, Vol. K-3, *North America and Adjacent Oceans During the Last Deglaciation*, edited by W.F. Ruddiman and H.E. Wright, pp. 111-135, Geol. Soc. of Am., Boulder, Colo., 1987.

Ochoa, J., and N.A. Bray, Water mass exchange in the Gulf of Cadiz, *Deep Sea Res., Part A, 38*, S465-S503, 1991.

Oppo, D.W., and R.G. Fairbanks, Atlantic Ocean thermohaline circulation of the last 150,000 years: Relation to climate and atmospheric CO_2, *Paleoceanography, 5*, 277-288, 1990.

Oppo, D.W., and S.J. Lehman, Mid-depth circulation of the subpolar North Atlantic during the last glacial maximum, *Science, 259*, 1148-1152, 1993.

Roemmich, D., and C. Wunsch, Two transatlantic sections: Meridional circulation and heat flux in the subtropical North Atlantic Ocean, *Deep Sea Res., Part A, 32*, 619-664, 1985.

Ruddiman, W.F., and A. McIntyre, Ice-age thermal response and climatic role of the surface Atlantic ocean, 40°N to 63°N, *Geological Society of America Bulletin, 95*, 381-396, 1984.

Sarnthein, M., K. Winn, J-C. Duplessy, and M. R. Fontugne, Global variations of surface ocean productivity in low and mid latitudes: Influences on CO_2 reservoirs of the deep ocean and atmosphere during the last 21,000 years, *Paleoceanography, 3*, 361-399, 1988.

Sarnthein, M., K. Winn, S.J.A. Jung, J-C. Duplessy, L. Labeyrie, H. Erlenkeuser, and G. Ganssen, Changes in east Atlantic deepwater circulation over the last 30,000 years: Eight time slice reconstructions, *Paleoceanography, 9*, 209-267, 1994.

Shackleton, N.J., Attainment of isotopic equilibrium between ocean water and the benthonic foraminiferal genus Uvigerina, isotopic changes in the ocean during the last glacial, *Colloq. Int. Cent. Nat. Rech. Sci., 219*, 203-219, 1974.

Slowey, N.C., and W.B. Curry, Enhanced ventilation of the North Atlantic subtropical gyre thermocline during the last glaciation, *Nature, 358*, 665-668, 1992.

Stommel, H., and A.B. Arons, On the abyssal circulation of the world ocean, I, Stationary planetary flow patterns on a sphere, *Deep Sea Res., 6*, 140-154, 1960a.

Stommel, H., and A.B. Arons, On the abyssal circulation of the world ocean, II, An idealized model of the circulation pattern and amplitude in oceanic basins, *Deep Sea Res., 6*, 217-233, 1960b.

Wunsch, C., The North Atlantic general circulation west of 50°W determined by inverse methods, *Rev. Geophys., 16*, 583-620, 1978.

Wunsch, C., Can a tracer field be inverted for velocity?, *J. Phys. Oceanogr., 15*, 1521-1531, 1985.

Wunsch, C., Tracer inverse problems, in *Oceanic Circulation Models: Combining Data and Dynamics*, edited by D.L.T. Anderson and J. Willebrand, pp. 1-77, Kluwer Acad., Norwell, Mass., 1989.

Zahn, R., and A.C. Mix, Benthic foraminiferal $\delta^{18}O$ in the ocean's temperature-salinity-density field: Constraints on Ice Age thermohaline circulation, *Paleoceanography, 6*, 1-20, 1991.

P. LeGrand, Laboratoire de Physique des Océans, IFREMER, Centre de Brest, BP 70, 29280, Plouzané, France. (e-mail: plegrand@ifremer.fr)

C. Wunsch, Center for Meteorology and Physical Oceanography, Department of Earth, Atmospheric, and Planetary Sciences, Massachusetts Institute of Technology, Cambridge, MA 02139. (e-mail: cwunsch@pond.mit.edu)

(Received July 20, 1994; revised May 8, 1995;
accepted May 8, 1995.)